

國立臺灣大學工學院土木工程學系

博士論文

Department of Civil Engineering

College of Engineering

National Taiwan University

Doctoral Dissertation

受剪混凝土柱之單軸循環桁架模型

Uniaxial Cyclic Truss Model of Reinforced Concrete Columns

Under Shear

林家宏

Lin, Chia-Hung

指導教授：羅俊雄 教授

Major Professor: Loh, Chin-Hsiung

中華民國 101 年 6 月



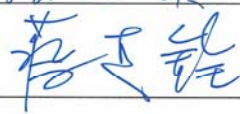

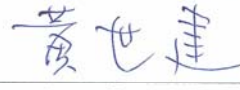


Jun. 2012

國立臺灣大學博士學位論文
口試委員會審定書

受剪混凝土柱之單軸循環桁架模型
Uniaxial Cyclic Truss Model of Reinforced Concrete Columns
Under Shear

本論文係林家宏君 (D91521009) 在國立臺灣大學土木工程學系
博士班完成之博士學位論文，於民國 101 年 6 月 20 日承下列考試委員
審查通過及口試及格，特此證明

口試委員：

羅 俊 雄	
(指導教授)	
張 國 鎮	
蔡 克 銓	
蔡 益 超	
黃 世 建	
黃 震 興	
系主任 呂 良 正	

誌謝

能完成這篇論文，我要特別感謝我的指導教授羅俊雄老師、我的指導委員張國鎮老師、黃世建老師、黃震興老師、蔡克銓老師、蔡益超老師、陳賢銘學長、吳俊霖博士。以及感謝指導過我的教授和各期同儕趙書賢、盧恭君、林威廷、李冠霈等每一位成員、朋友、家人對我的支持與鼓勵，謝謝大家。



中文摘要

本論文開發一單軸循環桁架模型用以預測鋼筋混凝土柱承受循環剪力之實際行為。經由應用物件導向程式設計，使用者可輕鬆將本模型與現有撓曲分析程式碼結合用以分析鋼筋混凝土柱承受軸力、撓曲、剪力時的複雜行為。單軸循環桁架模型分析結果將會反覆載重實驗結果比對結果成功預測破壞模式與遲滯行為。除此之外，本研究另開發一簡易預測模式用以直接快速預測鋼筋混凝土柱的破壞模式。此模式估測鋼筋混凝土柱的剪力容量並將之與側推分析得到的撓曲容量比較藉以決定其破壞模式。

關鍵字：單軸循環桁架模型、鋼筋混凝土柱、剪力



ABSTRACT

A uniaxial cyclic truss model (UCTM) is developed to simulate the hysteretic behavior of reinforced concrete columns under cyclic shear. Object-oriented programming methods are used to combine the proposed UCTM easily with any other developed flexural analysis methods to predict the response of RC columns under axial-flexural-shear loading. Analytical results obtained using UCTM are compared with the test result of reinforced concrete column specimens subjected to cyclic loading. It is shown that the UCTM can successfully predict the failure mode of a reinforced concrete column. Hysteretic relationships in UCTM can agree satisfactorily with experimental data. This thesis also proposes a simplified procedure to predict the failure mode of RC columns rapidly. The procedure is to evaluate the nominal shear strength of an RC column by UCTM and compares it to its peak lateral force that is obtained from pushover analysis, and thereby determines its failure mode.

Keywords: UCTM, Uniaxial cyclic truss model, Reinforced Concrete, RC column, Shear

CONTENTS

口試委員會審定書	i
誌謝	ii
中文摘要	iii
ABSTRACT	iv
CONTENTS	v
LIST OF FIGURES	viii
LIST OF TABLES	xi
Chapter 1 Introduction.....	1
1.1 History and Background of Shear Analysis.....	1
1.2 Summary of Shear Prediction.....	3
1.2.1 1 point shear value	4
1.2.2 Uniaxial linear shear analysis.....	4
1.2.3 Multiaxial linear shear analysis.....	4
1.2.4 Uniaxial nonlinear shear analysis.....	5
1.2.5 Multiaxial nonlinear shear analysis.....	5
1.3 Research Significance.....	5
Chapter 2 Uniaxial Cyclic Truss Model.....	7
2.1 Analytical Method	7
2.1.1 Brief introduction to truss model	7
2.1.2 Concept of uniaxial cyclic truss model (UCTM).....	7
2.2 Uniaxial Cyclic Truss Model.....	8
2.3 Solution Techniques.....	10
2.3.1 Dimensions of elements	10

2.3.2	Displacement field, degrees of freedom, strain field, and uniaxial strain/stress	11
2.3.3	Tangent stiffness.....	13
2.3.4	Shear Force.....	15
2.3.5	Defining column section using UCTM.....	15
Chapter 3	Objective-Oriented Programming Methods.....	16
3.1	Open System for Earthquake Engineering Simulation (OpenSees).....	16
3.2	Introduction to the Tcl command language	16
3.3	OpenSees Interpreter	17
3.4	Applying UCTM using OpenSees [14]	17
3.4.1	Introducing a new material into OpenSees	17
3.4.2	Material Abstractions	17
3.4.3	UniaxialMaterial Interface	19
3.5	Combining UCTM with Fiber Element Method	24
3.6	Materials For Building UCTM.....	25
3.6.1	Steel.....	25
3.6.2	Concrete	25
3.7	Hysteretic Characteristics Of Uniaxial Cyclic Truss Model	28
Chapter 4	Comparisons Of UCTM With Experiments.....	30
4.1	SY AND LY	30
4.2	N18C.....	30
4.3	H-19 AND F-19	31
4.4	BMRS	31
4.5	BMR2 (FLEXURAL FRACTURE DOMINATED)	31
Chapter 5	Predicting Failure Behavior of Reinforced Concrete Columns	

Subjected to Cyclic Loading	33
5.1 Shear Capacity of an RC Column.....	33
5.2 Flexural Capacity.....	37
5.3 Failure Mode Prediction	37
Chapter 6 Conclusions	39
REFERENCE	41

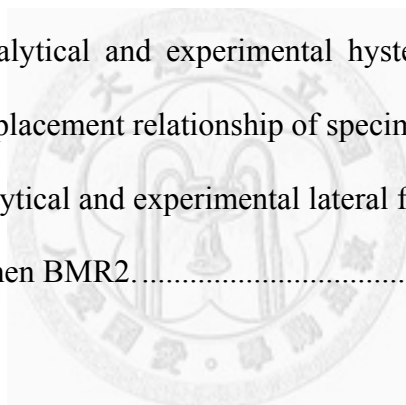


LIST OF FIGURES

Fig. 1–A parametric model simulating failure behavior of an RC column	51
Fig. 2–The truss mechanism of strut and tie model.....	52
Fig. 3–D zone and B zone of strut and tie model	53
Fig. 4–Comparison of analytical and experimental shear strength	54
Fig. 5–Comparison of normalized analytical and experimental shear strength	55
Fig. 6–Lateral View of experimental configuration of a shaking table test specimen. ...	56
Fig. 7–Analytical prediction of relationship between lateral force and displacement of a shaking table test specimen	57
Fig. 8–Truss model of a cantilever beam subjected to lateral force.	58
Fig. 9–Typical fracture mode of RC column in cyclic test: (a) Flexural failure (b) Shear failure.....	59
Fig. 10–RC column subjected to lateral force on top and bottom.	60
Fig. 11–Equilibrium diagrams of internal forces in UCTM (undeformed).....	61
Fig. 12–Equilibrium diagrams of internal forces in UCTM (deformed).....	62
Fig. 13–Components of internal forces in UCTM.....	63
Fig. 14–Equilibrium diagrams of shear forces in UCTM.....	64
Fig. 15–Uniaxial cyclic truss model (UCTM).....	65
Fig. 16–Projected area of the concrete struts in the direction parallel to DE onto the transverse steel element CD.	66
Fig. 17–Schematic drawing of “Section Aggregator”.....	67
Fig. 18–Application of UCTM to a RC column.....	68
Fig. 19–Concrete02 [17].....	69

Fig. 20–ReinforcingSteel [17]	70
Fig. 21–Core and cover concrete.....	71
Fig. 22–Lateral view of experimental configuration.....	72
Fig. 23–Analytical prediction of relationship between shear force and rotational angle- Section A1.....	73
Fig. 24–Analytical prediction of relationship between shear force and rotational angle- Section A2.....	74
Fig. 25–Analytical prediction of relationship between shear force and rotational angle- Section B1.....	75
Fig. 26–Analytical prediction of relationship between shear force and rotational angle- Section B2.....	76
Fig. 27–Framework of OpenSees.....	77
Fig. 28–Material class hierarchy. [14].....	78
Fig. 29–Flexural and shear models connected in series.....	79
Fig. 30–Comparison of analytical and test results for specimen SY.....	80
Fig. 31–Comparison of analytical and test results for specimen LY.....	81
Fig. 32–Comparison of analytical and test results for specimen N18C.....	82
Fig. 33–Comparison of analytical and test results for specimen H-19.....	83
Fig. 34–Comparison of analytical and test results for specimen F-19.....	84
Fig. 35–Lateral View of experimental configuration of specimen BMRS.....	85
Fig. 36–Comparison of analytical and experimental hysteretic loops associated with lateral force-displacement relationship of specimen BMRS for cycles 1-2: (a) cycle 1 (b) cycle 2.....	86
Fig. 37–Comparison of analytical and experimental hysteretic loops associated with lateral force-displacement relationship of specimen BMRS for cycles 3-4: (a)	

cycle 3 (b) cycle 4.....	87
Fig. 38–Comparison of analytical and experimental hysteretic loops associated with lateral force-displacement relationship of specimen BMRS for cycles 5-6: (a) cycle 5 (b) cycle 6.....	88
Fig. 39–Comparison of analytical and experimental hysteretic loops associated with lateral force-displacement relationship of specimen BMRS for cycles 7-8: (a) cycle 7 (b) cycle 8.....	89
Fig. 40–Comparison of analytical and experimental hysteretic loops associated with lateral force-displacement relationship of specimen BMRS for cycles 9-10: (a) cycle 9 (b) cycle 10.	90
Fig. 41–Comparison of analytical and experimental hysteretic loops associated with lateral force-displacement relationship of specimen BMRS for cycle 11. ...	91
Fig. 42–Comparison of analytical and experimental lateral force-displacement hysteretic loops for specimen BMR2.....	92



LIST OF TABLES

Table 1–Assumed input parameters of “ReinforcingSteel” material.....	44
Table 2–Assumed input parameters of “Concrete02” material	45
Table 3–Properties of cross-sections of the RC column.....	46
Table 4–Material properties of all specimens.....	47
Table 5–Sectional properties and calculated strength of core concrete.....	48
Table 6–Failure predicted by simplified UCTM	49
Table 7–Failure predicted by simplified UCTM	50



Chapter 1 Introduction

1.1 History and Background of Shear Analysis

The prediction of failure modes associated with shear have been concerned for decades. Unlike flexural failure which involves saturated hysteretic loops under cyclic loading, shear failure involves severe pinching, which dissipated less hysteretic energy. Determining whether RC columns will fail by flexure or shear is difficult. Traditional parametric model simulating an RC column as shown in Fig. 1 can not clearly distinguishing it. Various factors will cause shear failure. Many researchers have developed various methods for analyzing the response of an RC column under cyclic loading. However, most of them are limited by the restriction that the corresponding failure mode must be predetermined so that the analysis can then be performed under the presumed conditions. Methods such as finite element method are more comprehensive but the obtained results are not always satisfactory. Consequently, models such as the strut and tie model [1] had been developed to predict the responses of RC columns as shown in Fig. 2 and Fig. 3. Such methods enabled RC columns to be analyzed without the need to presume the failure mode in advance.

For simplicity, the elastic response of a reinforced concrete column can be conceptually divided into the axial, flexural, and shear responses. In nonlinear numerical analysis, this division yields valid approximate solution in incremental form. The cyclic inelastic axial and flexural analyses have been extensively developed for application to analyzing and designing RC columns. Whereas flexural analysis has been well established, theories of RC columns under shear are lacking. The flexural capacity of a column can be approximated from given sectional and material properties. But it is difficult to understand the behavior of RC columns under shear.

Shear analysis is multiaxial in either 2D or 3D coordinates. The shear analysis of structures was frequently simplified by treating the problem as a plane stress problem, even though in reality, the system has three degrees of freedom including longitudinal, lateral, and shear rotational directions. Multiaxial analysis, like the finite element method, provides high accuracy but is rather computationally intensive.

To overcome the difficulty of solid mechanical analysis, shear theories assuming average stress-strain relationship had been proposed. Modified compression field theory (MCFT) [2] based on compression field theory (CFT) [3] had successfully been used to evaluate the shear performance of beams and shear walls, and had formed the basis of various methods presented subsequently. Similar to CFT, the rotating-angle softened truss model (RA-STM) and the fixed-angle softened truss model (FA-STM) predicted the prepeak ascending shear forces, neglecting the Poisson's ratio [4]. The softened membrane model (SMM) [4, 5] was developed to predict postpeak descending branch of shear force using the new Poisson's ratio (Hsu/Zhu ratio). Subsequently, the cyclic softened membrane model (CSMM) [6] derived from the softened membrane model (SMM) [4] improved upon SMM by including a cyclic shear analysis, rather than a monotonic. The model had been accurately utilized to shear walls and hollow columns under the plane stress assumption. Shear models that took a global view of a structural member had also been proposed. For example, Mo [7] developed an analytical model of cyclic shear that statically and dynamically predicted the shear force-deflection behavior of shear walls. A hysteretic shear model that established a primary envelope curve using compression field theory [8] had also been proposed to determine shear force-deformation relationship of RC members. The relevant parameters were obtained using regression approaches. Such a parametric model was relatively convenient, although some of its assumptions limited its use. The model was limited to structural members

that yield in flexure prior to shear failure and no attempt was made to define the response beyond the onset of strength decay [8].

On the other hand, few structural programs are available that provide a shear model for sectional analysis in situations in which a uniaxial relationship exists between shear force and rotational angle. Only some of the programs supported a user-defined nonlinear sectional uniaxial shear relationship. The users can input basic parameters, including the values of shear stiffness and strength in the initial, post-yield, post peak, and residual stages. These shear models are easy to be used in programs, but the corresponding parameters are difficult to decide. In sectional analysis in practice, the shear response is commonly either neglected or presumed to be linear.

Cyclic behaviors of RC columns under shear are problematic. Based on the well known truss model [9, 10], a uniaxial cyclic truss model (UCTM) is developed in this paper to simulate an RC column. The proposed UCTM condenses three degrees of freedom into one. Shear rotation is the only degree of freedom that is preserved. This method isolates the shear behavior of a column from flexural and axial behaviors.

In traditional flexural analysis, one cross section yields one hysteretic relationship. Similarly, UCTM converts the sectional and material properties to a uniaxial hysteretic relationship between the shear force and the angle of rotation. To verify the proposed procedure, the analytical results obtained by UCTM are compared with the experimental results of seven specimens from different laboratories.

1.2 Summary of Shear Prediction

Shear analysis can be grouped into 5 groups according to linearity, loading paths, and uniaxial or multiaxial stress-strain (or force-deformation) relationships.

1.2.1 1 point shear value

For decades, ultimate shear strength of an RC element is calculated to evaluate the shear capacity. Most of them calculate the summation of shear strength contributed by concrete and transverse reinforcing steels. This value is independent with loading paths. In this case, shear stiffness is neither calculated. This method are mostly assumed by building codes such as ACI building codes [1] to evaluate shear capacity of an RC column. Fig. 4 shows 11 kinds of calculated results of 1 point shear values using different methods compared with 9 experimental results [11]. The calculated results using these methods are not always trusted. The error may up to near 200% as shown in Fig. 5. It shows the difficulty of shear capacity prediction. The existing method shows huge deviation even for only 1 point calculation of ultimate shear value. Of course the monotonic and hysteretic behaviors have not been considered yet in this case.

1.2.2 Uniaxial linear shear analysis

Shear stiffness can be considered rigid compared to flexural stiffness. This is also the hypothesis of Euler beam in elasticity. However, some researchers intend to consider shear stiffness in RC element analysis to increase the total accuracy. In this case, the loading path can be either monotonic or cyclic. Because only 1-D stress-strain (or force-deformation) relationship is considered, it is uniaxial. The only parameter is shear stiffness. In general, this parameter is difficult to be relevantly decided.

1.2.3 Multiaxial linear shear analysis

The nature of shear is multiaxial. As can be seen in Mohr's circle, 2 principle values are necessary to be calculated to decide shear in one point in 2-D analysis, while it is 3 in 3-D analysis. This method is mostly adopted in linear finite element analysis. This can be done in monotonic or cyclic loading paths. But the accuracy is often doubtful.

1.2.4 Uniaxial nonlinear shear analysis

The ideal method to analyze shear is to analyze it as flexural analysis. The development of nonlinear flexural analysis of an RC beam-column element is mature and accurate for applying in practice during these years. Even for a complex shaking table test as shown in Fig. 6, the flexural analysis using fiber element analysis gives accurate prediction. The result is shown in Fig. 7. The flexural stiffness of an RC beam-column element can be decided for each nonlinear steps in nonlinear analysis without difficulty. For each rotational angle of the RC column a corresponding flexural stiffness can be obtained to accomplish the nonlinear analysis step by step. But it is not true for shear. Because shear is decided from two principle values of axial forces, it can not be readily obtained from one given value of rotational angle in RC column analysis. Besides, RC column analysis is inhomogeneous and nonisotropic. Few researcher focus on this part. The proposed method UCTM dealt it.

1.2.5 Multiaxial nonlinear shear analysis

Multiaxial nonlinear shear analysis is to consider shear as nonlinear and in multiaxial directions of stress-strain (or force-deformation) relationships. It seems to be the most rigorous and reliable method to analyze shear in an RC column. Generally it is accomplished by nonlinear finite element method. Most researchers invented their life to develop shear analysis method in this type. Simulations of an RC column subjecting to monotonic or cyclic loading paths can be done by this kind of method.

1.3 Research Significance

Many of the existing methods for evaluate the response of an RC column under cyclic loading depend on the predetermination of the failure mode. Although some approaches did not meet this problem, but most among these involve a meshing procedure to

establish an analytical model. This study proposes an alternative way to predict the cyclic shear behavior of an RC column for given cross-sectional properties. The total cyclic response of an RC column can be determined using this method without a priori knowledge of failure mode.



Chapter 2 Uniaxial Cyclic Truss Model

2.1 Analytical Method

2.1.1 Brief introduction to truss model

The truss model was introduced in 1899 [9, 10]. The flexural behavior was modeled primarily by the chord under tension on the top and the chord under compression at the bottom as shown in Fig. 8. The tensile chord represented main steel and the compressive chord represented concrete under compression. Transverse reinforcement provides vertical members and concrete between inclined cracks act as 45° compression diagonal members [12]. The shear force was calculated as a sum of contributions from concrete and transverse reinforcement. However, in the original truss model the analysis was in monotonic and the concrete was not under tension.

Cyclic analysis has become essential recently, as the monotonic analysis can not satisfy practical requirements. Many literatures showed that the tension in concrete is important in shear [2, 4, 6]. Flexural analysis performed using the truss model was rather incomplete, so more accurate models such as the fiber element method [13] soon replace it. Based on the original concept of truss model, the UCTM proposed in this paper overcomes these shortcomings.

2.1.2 Concept of uniaxial cyclic truss model (UCTM)

Incremental deformation in a nonlinear numerical analysis of an RC column can be divided into a flexural part, which includes an axial part, and a shear part, as shown in Fig. 9, which plots the hysteretic loops of columns that are dominated by flexure and shear, respectively. In Fig. 9(a), saturated hysteretic loops are associated with flexural behavior. In contrast, columns that are dominated by shear exhibit severe pinching, as displayed in Fig. 9(b). In this paper, the shear part is simulated using the proposed

uniaxial cyclic truss model while the flexural part is simulated using fiber element method under the platform OpenSees [14].

2.2 Uniaxial Cyclic Truss Model

Consider the RC column shown in Fig. 10 that is subjected to shear deformation in static equilibrium. The corresponding shear behavior was analyzed in an average sense under small shear deformations that results from lateral loadings on top and bottom of the column. Elements AG and BH represent vertical components of the RC column that are subjected to vertical axial loads and moments. These flexural components, comprising longitudinal steel bars and concrete, can be simulated using any methods in flexural analysis. Hence, elements AG and BH are assumed to be rigid in UCTM for shear analysis.

Elements AB, CD, EF, and GH are transverse reinforcement elements while elements AD, CF, and EH are concrete elements under compressive forces, and BC, DE, and FG are concrete elements under tensile forces. With reference to the free body diagram of element CDFE in Fig. 11, shear deformation will cause vertical elements CE and DF to rotate rigidly without bearing horizontal shear forces.

The external forces are applied at both ends of the column. Since no other lateral load acts upon the mid-portion of this column, the entire column is subjected to uniform shear force and deformation. So for the column considered, the behavior of all rectangular elements, such as ABDC, CDFE, and EFHG in Fig. 10, can be reasonably assumed to be identical. Therefore, a unique uniaxial shear hysteretic model can be derived from given cross-sectional parameters.

Consider element CDFE in Fig. 11 subjected to internal axial forces exerted by adjacent elements immediately above and below it. Since elements ABDC, CDFE, and EFHG in

Fig. 10 are identical,

$$F_{AD} = F_{CF} = F_{EH} \quad (1a)$$

$$F_{BC} = F_{DE} = F_{FG} \quad (1b)$$

where F_{AD} , F_{CF} , F_{EH} , F_{BC} , F_{DE} , and F_{FG} are internal axial force in element AD, CF, EH, BC, DE, and FG, respectively.

Assume that the free body element CDFE subjected to F_{BC} , F_{AD} , F_{FG} , and F_{EH} , eventually deforms to the state as shown in Fig. 11 Fig. 12 and rotates by an angle γ .

The external forces shown in Fig. 12 are decomposed into horizontal and vertical components in local coordinate, as shown in Fig. 13. The component forces satisfy the following relationships.

$$V_{AD} = F_{AD} \cos \alpha = V_{CF} = F_{CF} \cos \alpha = V_{EH} = F_{EH} \cos \alpha \quad (2a)$$

$$V_{BC} = F_{BC} \cos \alpha = V_{DE} = F_{DE} \cos \alpha = V_{FG} = F_{FG} \cos \alpha \quad (2b)$$

$$N_{AD} = F_{AD} \sin \alpha = N_{CF} = F_{CF} \sin \alpha = N_{EH} = F_{EH} \sin \alpha \quad (2c)$$

$$N_{BC} = F_{BC} \sin \alpha = N_{DE} = F_{DE} \sin \alpha = N_{FG} = F_{FG} \sin \alpha \quad (2d)$$

where

α = angle DEF, equals to angle CFE for small rotational angle γ ,

V_{AD} , V_{CF} , V_{EH} , V_{BC} , V_{DE} , and V_{FG} are horizontal component of F_{AD} , F_{CF} , F_{EH} , F_{BC} , F_{DE} , and F_{FG} , respectively.

N_{AD} , N_{CF} , N_{EH} , N_{BC} , N_{DE} , and N_{FG} are vertical component of F_{AD} , F_{CF} , F_{EH} , F_{BC} , F_{DE} , and F_{FG} , respectively.

In this model, vertical rigid elements CE and DF are assumed to sustain the axial and flexural forces.

In the following section, the shear mechanism is simulated by treating element CDFE as

an internal structure that is subjected to shear deformation. In Fig. 11Fig. 14, the shear deformation in the uniaxial cyclic truss model causes a rotation by angle γ , determined by the components of shear force on four edges of element CDFE. The total shear force on section CD and EF are identical:

$$V = -V_{CF} + V_{DE} \quad (3)$$

Where V denotes total shear force.

V can be determined for a given value of γ . It can be evaluated using nonlinear structural solving schemes.

2.3 Solution Techniques

Details of solution procedures of the UCTM to determine the shear force for any γ are presented below.

2.3.1 Dimensions of elements

First, the sizes of the concrete and steel elements in Fig. 15 is determined. The body of the UCTM comprises core concrete and transverse reinforcement. The cover concrete is generally too brittle to carry shear force and thus is not considered. With reference to Fig. 10 and Fig. 15, the undeformed length of CD and EF are d_c . The undeformed length of CF and DE are $d_c \tan \alpha$, obtained geometrically.

The areas of the cross-sections of the elements is also determined. The areas of the cross-section of the steel elements CD and EF are their actual areas of transverse reinforcement in the x-z plane within spacing s .

$$A_{CD} = A_{EF} = \rho_y b_c d_c \tan \alpha \quad (4)$$

The areas of the cross-section of the concrete elements CF and DE are also calculated to formulate tangent stiffness equations. Fig. 16 displays the diagonal concrete struts, which are simulated as the diagonal element DE. The total projected area of the

concrete struts in the direction parallel to DE onto the transverse steel element CD is

$$A_{DE} = \int_{z=0}^{z=d_c \tan \alpha} dA \cos \alpha = \cos \alpha \int_{z=0}^{z=d_c \tan \alpha} b_c dz = b_c d_c \tan \alpha \cos \alpha = b_c d_c \sin \alpha \quad (5a)$$

where

z = distance along vertical axis from point E, shown in Fig. 16.

Similarly,

$$A_{CF} = A_{DE} = b_c d_c \sin \alpha \quad (5b)$$

2.3.2 Displacement field, degrees of freedom, strain field, and uniaxial strain/stress

Throughout this paper, generalized degrees of freedom, known as generalized coordinates [15], Δ_1 and Δ_2 are used. The displacement field that is applied to UCTM is stated in terms of Δ_1 and Δ_2 by the equation

$$\begin{pmatrix} v \\ w \end{pmatrix} = \begin{pmatrix} \Delta_1 - \Delta_2 + \frac{\Delta_2 - \Delta_1}{d_c} y + \frac{\Delta_2}{d_c \tan \alpha} z \\ 0 \end{pmatrix} \quad (6)$$

where

y, z = rectangular Cartesian coordinates in the undeformed state shown in Fig. 15, and

v, w = components of displacement in the y , and z directions, respectively.

In Fig. 15, the UCTM is displayed in the deformed state which is shown in Fig. 11 Fig. 14. Edges C, D, and E are modeled as roll supports while edge F is hinge-supported. The displacement field of such a 2D structural problem has three degrees of freedom. However, as mentioned previously, element CE and DF are rigid. Accordingly, only two degrees of freedom remain. Δ_1 refers to lateral deformation, or expansion and contraction. Δ_2 is constrained to γ , which denotes the shear rotational angle,

$$\Delta_2 = \gamma d_c \tan \alpha \quad (7)$$

Hence, the strain field that is associated with the displacement gradient components is

$$\boldsymbol{\varepsilon} = \begin{bmatrix} \frac{\partial v}{\partial y} & \frac{1}{2} \left(\frac{\partial v}{\partial z} + \frac{\partial w}{\partial y} \right) \\ \frac{1}{2} \left(\frac{\partial w}{\partial y} + \frac{\partial v}{\partial z} \right) & \frac{\partial w}{\partial z} \end{bmatrix} = \begin{bmatrix} \frac{\Delta_2 - \Delta_1}{d_c} & \frac{\Delta_2}{2d_c \tan \alpha} \\ \frac{\Delta_2}{2d_c \tan \alpha} & \mathbf{0} \end{bmatrix} \quad (8)$$

The uniaxial strain in a direction parallel to $\mathbf{n} = [\cos \theta, \sin \theta]^T$ is

$$\varepsilon_\theta = \mathbf{n}^T \boldsymbol{\varepsilon} \mathbf{n} = [\cos \theta, \sin \theta] \begin{bmatrix} \frac{\Delta_2 - \Delta_1}{d_c} & \frac{\Delta_2}{2d_c \tan \alpha} \\ \frac{\Delta_2}{2d_c \tan \alpha} & \mathbf{0} \end{bmatrix} \begin{bmatrix} \cos \theta \\ \sin \theta \end{bmatrix} \quad (9)$$

For $\theta = \mathbf{0}$, in the direction parallel to element CD,

$$\varepsilon_\theta = \frac{\Delta_2 - \Delta_1}{d_c} \quad (10a)$$

For $\theta = \alpha$, in the direction parallel to element DE,0

$$\varepsilon_\theta = \frac{2\Delta_2 - \Delta_1}{d_c} \cos^2 \alpha \quad (10b)$$

For $\theta = \pi - \alpha$, in the direction parallel to element CF,

$$\varepsilon_\theta = \frac{-\Delta_1}{d_c} \cos^2 \alpha \quad (10c)$$

From Equation (10a, b, c), a change of the uniaxial stress caused by changes of Δ_1 and Δ_2 of any truss member is given by

$$d\sigma_{CD} = C_{CD} \frac{d\Delta_2 - d\Delta_1}{d_c} \quad (11a)$$

$$d\sigma_{DE} = C_{DE} \frac{2d\Delta_2 - d\Delta_1}{d_c} \cos^2 \alpha \quad (11b)$$

$$d\sigma_{CF} = C_{CF} \frac{-d\Delta_1}{d_c} \cos^2 \alpha \quad (11c)$$

where C denotes the corresponding tangent modulus. Subscripts refer to elements CD, CF, and DE. Notably, the behavior of element EF is identical to element CD.

2.3.3 Tangent stiffness

The tangent stiffness in UCTM is the derivative of the total shear force V with respect to the rotational angle γ . Since the total shear force is given by Equation (3), the change of V equals the change of the horizontal projection of the axial forces of element CF and DE caused by changes of Δ_1 and Δ_2 . According to Equation (3),

$$dV = -dV_{CF} + dV_{DE} \quad (12)$$

where, from Equation (2a, b)

$$dV_{CF} = dF_{CF} \cos \alpha \quad (13a)$$

$$dV_{DE} = dF_{DE} \cos \alpha \quad (13b)$$

Applying Equation (4, 5, 11) yields the axial force in truss members, as follows.

$$dF_{CD} = d\sigma_{CD} A_{CD} = \rho_y C_{CD} (d\Delta_2 - d\Delta_1) b_c \tan \alpha \quad (14)$$

$$dF_{DE} = d\sigma_{DE} A_{DE} = C_{DE} (2d\Delta_2 - d\Delta_1) b_c \cos^2 \alpha \cdot \sin \alpha \quad (15)$$

$$dF_{CF} = d\sigma_{CF} A_{CF} = -C_{CF} d\Delta_1 b_c \cos^2 \alpha \cdot \sin \alpha \quad (16)$$

The horizontal equilibrium of any of the points C, D, E, or F yields the relationship between $d\Delta_1$ and $d\Delta_2$,

$$dF_{CD} + dF_{DE} \cos \alpha + dF_{CF} \cos \alpha = 0 \quad (17)$$

$$d\Delta_1 = \frac{\rho_y C_{CD} + 2\cos^4 \alpha C_{DE}}{\rho_y C_{CD} + \cos^4 \alpha C_{DE} + \cos^4 \alpha C_{CF}} d\Delta_2 \quad (18)$$

Differentiating Equation (7) yields

$$d\Delta_2 = d_c \tan \alpha d\gamma \quad (19)$$

Substituting these equations into Equation (12) and factorizing yields,

$$dV = \frac{(C_{CD}C_{DE} \cos^2 \alpha \cdot \sin^2 \alpha + C_{CD}C_{CF} \cos^2 \alpha \cdot \sin^2 \alpha)\rho_y + 4C_{CF}C_{DE} \cos^6 \alpha \cdot \sin^2 \alpha}{C_{CD}\rho_y + C_{DE} \cos^4 \alpha + C_{CF} \cos^4 \alpha} b_c d_c d\gamma$$

$$= Kd\gamma$$
(20)

where

$$K = \frac{(C_{CD}C_{DE} \cos^2 \alpha \cdot \sin^2 \alpha + C_{CD}C_{CF} \cos^2 \alpha \cdot \sin^2 \alpha)\rho_y + 4C_{CF}C_{DE} \cos^6 \alpha \cdot \sin^2 \alpha}{C_{CD}\rho_y + C_{DE} \cos^4 \alpha + C_{CF} \cos^4 \alpha} b_c d_c$$
(21)

K = tangent stiffness of UCTM.

In case the concrete and steel remain elastic and the tension in the concrete is omitted, then

$$C_{CD} = E_s$$
(22a)

$$C_{CF} = E_c$$
(22b)

$$C_{DE} = 0$$
(22c)

Substituting Equation (32) into Equation (20) yields

$$K = \frac{E_s E_c \cos^2 \alpha \cdot \sin^2 \alpha \rho_y}{E_s \rho_y + E_c \cos^4 \alpha} b_c d_c = \frac{\rho_y n \cot^2 \beta}{1 + \rho_y n \csc^4 \beta} E_c A_c$$
(23)

where $n = E_s/E_c$ is the modular ratio, $A_c = b_c d_c$ and $\beta = 90^\circ - \alpha$. Equation (23) is a special case of UCTM that is equivalent to the equation for shear stiffness of a differential truss element, derived from constant angle truss model [16].

The crack angle α in the above equations must be determined. The shear crack angle varies somewhat between around 25° and 65° in a manner that depends on various factors [12]. However, an average of 45° was reasonably assumed for simplicity, consistent with the ACI code method [12]. It can be considered rotated in the future.

2.3.4 Shear Force

Equation (12) yields the incremental shear strength dV . Thus, the total shear force is

$$V = V_0 + dV \quad (24)$$

where

V_0 = total shear force in the previous step.

2.3.5 Defining column section using UCTM

In this paper the UCTM was incorporated into OpenSees platform. OpenSees utilizes a class that is called “Section Aggregator”, which adds another one degree of freedom associated with shear to a single section force-deformation model to allow shear behavior to be simulated, as shown in Fig. 17. The hysteretic behaviors of the cross-section of a beam-column element under flexure and axial loading can be computed using an independently developed method preferred. Fig. 18 presents procedures for applying UCTM in a cross-section in the analysis of a reinforced concrete column analysis. The implementation of UCTM on the OpenSees platform herein required only 5 parameters - f'_c , f_y , d_c , b_c , and ρ_y . UCTM can also be applied to non-prismatic RC columns. The cross-sectional dimensions and other properties can be varied along the longitudinal direction of a RC column.

Chapter 3 Objective-Oriented Programming

Methods

3.1 Open System for Earthquake Engineering Simulation (OpenSees)

This paper develops various classes and objects to build UCTM class under the platform OpenSees [17]. OpenSees is an object-oriented framework for finite element analysis. OpenSees' intended users are in the research community. A key feature of OpenSees is the interchangeability of components and the ability to integrate existing libraries and new components into the framework (not just new element classes) without the need to change the existing code as shown in Fig. 27. Core components, that is the abstract base classes, define the minimal interface (minimal to make adding new component classes easier but large enough to ensure all that is required can be accommodated).

3.2 Introduction to the Tcl command language

The Tcl scripting language [17, 18] was chosen to support the OpenSees commands, which are used to define the problem geometry, loading, formulation and solution. These commands are one-line commands which have specific tasks, as described in this manual. The Tcl language provides useful programming tools, such as variables manipulation, mathematical-expression evaluation and control structures.

Tcl is a string-based scripting language which allows the following:

- Variables and variable substitution
- Mathematical-expression evaluation
- Basic control structures (if, while, for, foreach)

- Procedures
- File manipulation

3.3 OpenSees Interpreter

The main abstractions of OpenSees will be explained using the OpenSees interpreter. The interpreter is an extension of the Tcl scripting language. The OpenSees interpreter adds commands to Tcl for finite element analysis. Each of these commands is associated (bound) with a C++ procedure that is provided. It is this procedure that is called upon by the interpreter to parse the command. In this document we outline only those commands which have been added to Tcl by OpenSees [17].

3.4 Applying UCTM using OpenSees [14]

Object-oriented programming methods are employed to establish the analytical model, UCTM. With object-oriented programming methods, UCTM can be constructed from various concrete and steel materials. The UCTM can also be made to be incorporated into various beam-column elements conveniently. The UCTM class is a derived class of “Material” class built in OpenSees.

3.4.1 Introducing a new material into OpenSees

The hierarchical nature of the OpenSees software architecture allows new material models to be seamlessly added to the framework. By keeping element and material implementations separate, a new material model can be used in an existing element without modifying the element implementation, and vice versa. The programming language C++ directly supports the data encapsulation and run-time binding necessary to achieve this complete separation of material from element. [14]

3.4.2 Material Abstractions

Currently, there are three Material abstractions in OpenSees, each of which can be used

across a wide range of element implementations:

1. `UniaxialMaterial` - Provides the interface for all one-dimensional material models, either stress-strain or force-deformation. `UniaxialMaterial` models define the stress-strain response of a truss element, uniaxial fiber behavior in a beam-column section, or the force-deformation response of a beam section or zero-length element.
2. `NDMaterial` - The multi-dimensional generalization of `UniaxialMaterial`; provides the stress-strain response at a point in a solid element, or multi-dimensional fiber behavior in a plate or beam-column section.
3. `SectionForceDeformation` - Defines the interface for stress resultant models which are used to describe both plate and beam-column force-deformation response as well as the constitutive response of more general zero-length elements, e.g., for isolator bearings.

Each interface listed above is essentially the same with minor differences. The `NDMaterial` and `SectionForceDeformation` abstractions both represent multi-dimensional constitutive response. However, a distinction is made between stress and stress resultant response to allow for safer element implementations. Furthermore, the stress-strain equations for continuum material models can be written in terms of tensors. This is not the case for stress resultant models. Lastly, to avoid returning matrices and vectors or tensors of size one, the `UniaxialMaterial` abstraction is made distinct for reasons of efficiency, as scalar values describe the behavior of a one-dimensional model. `UCTM` is inherited from class `UniaxialMaterial` modeling the force-deformation response of a RC column section.

As indicated in Fig. 28, each material abstraction is a subclass of `Material`. The `Material` class is a subclass of both the `TaggedObject` and `MovableObject` classes, and therefore inherits the functionality of these two classes. As a result, it can be said that a `Material`

“is a” TaggedObject as well as a MovableObject. Furthermore, since each of UniaxialMaterial, NDMaterial, and SectionForceDeformation “is a” Material, each is also a TaggedObject and a MovableObject. The TaggedObject class provides functionality for identifying materials, through a tag, during model building; and the MovableObject class provides functionality for parallel processing and database programming.

Rather than show examples of implementing a material model under each interface, only the UniaxialMaterial interface is covered herein. The basic concepts of adding a material model to OpenSees carry directly over from UniaxialMaterial to NDMaterial and Section-ForceDeformation. The remainder of this document is laid out as follows.

First, the UniaxialMaterial interface is listed and explained. Along with the C++ implementation, it is shown how to

1. add the new model to the OpenSees Tcl model builder, and
2. make the new model “movable” for parallel processing and database programming.

[14]

3.4.3 UniaxialMaterial Interface

Implementations of the UniaxialMaterial interface are used in several contexts within the OpenSees modeling framework. Due to their simplicity, these models can define both stress-strain and force-deformation relationships. It is up to the calling object, be it an element object or another material object, to interpret the meaning appropriately.

Listed below is the UniaxialMaterial class interface. All methods in the UniaxialMaterial interface are public, there are no protected or private data or methods. Following the UniaxialMaterial class interface listing, each method in the interface is described.

```
#include <Material.h>
```

```

class Response;

class Information;

class UniaxialMaterial : public Material
{
public:
    UniaxialMaterial(int tag, int classTag);

    virtual ~UniaxialMaterial(void);

    virtual int setTrialStrain(double strain, double strainRate = 0.0) = 0;

    virtual double getStrain(void) = 0;

    virtual double getStrainRate(void);

    virtual double getStress(void) = 0;

    virtual double getTangent(void) = 0;

    virtual double getDampTangent(void);

    virtual double getSecant(void);

    virtual int commitState(void) = 0;

    virtual int revertToLastCommit(void) = 0;

    virtual int revertToStart(void) = 0;

    virtual UniaxialMaterial *getCopy(void) = 0;

    virtual Response *setResponse(char **argv, int argc, Information &matInfo);

    virtual int getResponse(int responseID, Information &matInfo);

protected:

private:
};

```

A note about the C++ syntax seen in the UniaxialMaterial interface. The keyword “virtual” at the start of a method declaration indicates this method may be overridden by a

subclass of `UniaxialMaterial`. The `UniaxialMaterial` base class provides default implementations for its virtual methods. The notation “= 0” at the end of the method declaration indicates the method is pure virtual, meaning it must be defined by subclasses because the `UniaxialMaterial` base class does not provide a default implementation.

The `UniaxialMaterial` base class constructor takes a `tag` and `classTag` as its arguments.

The `tag` passed to the constructor identifies this `UniaxialMaterial` as unique among all other `UniaxialMaterial` objects, and the `classTag` is used primarily for parallel processing and database programming. Class tags are defined in the file `classTags.h`. The `tag` and `classTag` arguments are passed to the `Material` class constructor, where they are in turn passed to the `TaggedObject` and `MovableObject` class constructors, respectively.

The `UniaxialMaterial` destructor is declared, but does not do anything as the `UniaxialMaterial` base class contains no data.

The method `setTrialStrain()` takes one or two arguments, an updated strain and strain rate. The strain rate is an optional argument, with default value 0.0. This method is pure virtual, so it must be implemented in all subclasses of `UniaxialMaterial`. The next two methods, `getStrain()` and `getStrainRate()`, are to return the current strain and strain rate of this `UniaxialMaterial`. The method `getStrain()` is pure virtual, while `getStrainRate()` is only virtual; by default it returns 0.0, but may be overridden in subclasses if needed.

double

`UniaxialMaterial::getStrainRate(void)`

```
{  
    return 0.0;  
}
```

The next method is `getStress()`, which is to return the current stress of this `UniaxialMa-`

terial. The current stress is a function of the current strain, ε , and the current strain rate, $\dot{\varepsilon}$,

$$\sigma = \sigma(\varepsilon, \dot{\varepsilon}) \quad (25)$$

The `getStress()` method is pure virtual and must be implemented by subclasses of `UniaxialMaterial`.

The current material tangent is returned by the next method, `getTangent()`. The material tangent is the partial derivative of the material stress with respect to the current strain,

$$D_t = \frac{\partial \sigma}{\partial \varepsilon} \quad (26)$$

The `getTangent()` is also pure virtual and must be implemented in all `UniaxialMaterial` subclasses.

The `getDampTangent()` method is next, and is to return the current damping tangent, which is the partial derivative of the current stress with respect to the current strain rate,

$$\eta = \frac{\partial \sigma}{\partial \dot{\varepsilon}} \quad (27)$$

By default, this method returns 0.0, and it may be overridden in subclasses of `UniaxialMaterial` where there is strain rate dependence.

double

`UniaxialMaterial::getDampTangent(void)`

```
{  
  
    return 0.0;  
  
}
```

Finally, the `getSecant()` method is provided to return the material secant, which is the current stress divided by the current strain,

$$D_s = \frac{\sigma}{\varepsilon} \quad (28)$$

By default, this method returns the result of dividing the current stress by the current strain. If the current strain is zero, the current tangent is returned instead.

double

UniaxialMaterial::getSecant(void)

```
{
    double strain = this->getStrain();
    double stress = this->getStress();
    if (strain != 0.0)
        return stress/strain;
    else
        return this->getTangent();
}
```

The next set of methods deal with possible path dependent behavior of UniaxialMaterial models. All Material objects in OpenSees are responsible for keeping track of and updating their own history variables. First, the method `commitState()` is invoked to inform a UniaxialMaterial object that its current state is on the converged solution path and its internal history variables should be updated accordingly. Next, the method `revertToLastCommit()` is provided to let a UniaxialMaterial object know that it should return to its last committed state at. Finally, `revertToStart()` informs the UniaxialMaterial object to revert to its initial state, i.e., at the start of the analysis. All three of these methods are pure virtual, and thus must be implemented in all subclasses of UniaxialMaterial. The `getCopy()` method is declared so a calling object, be it an Element, Fiber, or another Material object, can obtain an exact copy of this

UniaxialMaterial object. A pointer to the new object is returned by this function, and the calling object is responsible for deleting this dynamically allocated memory. This method is pure virtual because only a subclass of UniaxialMaterial knows the internal representation of its data.

The final two methods, setResponse() and getResponse(), are declared for recording UniaxialMaterial state information. These methods have default implementations to record the material stress, strain, and tangent. These methods may be overridden, but their implementations are not shown in this thesis.

3.5 Combining UCTM with Fiber Element Method

The flexural response of an RC column is simulated using fiber element method while the shear response is simulated using UCTM in this paper. For fiber element analysis, a cross-section of an RC column can be divided into three parts – the concrete part, the cover concrete part, and the longitudinal steel part. The enhancement of the compressive strength and strain at ultimate compressive strength of core concrete by the confinement of transverse reinforcement is estimated using a theoretical stress-strain model for confined concrete [19]. The core concrete fiber is thus simulated as the “Concrete02” material implemented in OpenSees with tension. Since the cover concrete fiber is not confined by transverse reinforcement, it is simulated as the normal concrete material “Concrete01” in OpenSees [14] without tension for simplicity. The longitudinal steel fibers were simulated as the “ReinforcingSteel” material in OpenSees. To incorporate UCTM into fiber element, the object called “Section Aggregator” in OpenSees is used to add a degree of freedom associated with shear. UCTM is then used to determine the relationship between the shear force and rotational angle associated with this additional degree of freedom. This command is used to construct a SectionAggregator object

which aggregates groups previously-defined UniaxialMaterial objects into a single section force-deformation model. Each UniaxialMaterial object represents the section force-deformation response for a particular section degree-of-freedom (dof). There is no interaction between responses in different dof directions. The aggregation can include one previously defined section. The basic concept used in an aggregator is superposition. The flexural model and shear model can be treat connected in series as shown in

3.6 Materials For Building UCTM

UTCM can be fabricated from various concrete and steel uniaxial materials. In this study, two materials “Concrete02” and “ReinforcingSteel” were adopted in OpenSees [17] as the materials of the elements in UCTM. The corresponding hysteretic behaviors are displayed in Fig. 19 and Fig. 20 These material models can be changed to others if required.

3.6.1 Steel

Transverse steel bar elements comprise the “Reinforcing” uniaxial steel material in the OpenSees platform. Table 1 lists the necessary input parameters [17]. In case ties are present, the properties of the tie material are assumed to be the same as those of the hoop material for conservation and for convenience. The other parameters can be estimated using the equations that are presented in Table 1.

3.6.2 Concrete

Various uniaxial concrete models have been developed in recent years. However, this paper adopts uniaxial concrete material “Concrete02” from OpenSees platform. Table 2 presents material parameters that are required to establish a Concrete02 object [17].

The concrete in reinforced concrete columns can be classified as cover concrete and core concrete as displayed in Fig. 21. The core concrete, which is confined by hoop

steels, has a substantially higher strength and toughness of concrete. Different methods had been proposed to take into account the effects of confinement. However, the theoretical stress-strain model for confined concrete with the application of the multi-axial failure criterion [19] was found to be particularly effective to conduct any type of confining steels. Therefore, the considerable increase in both f'_c and ϵ_{co} owing to confinement of concrete must be accounted for by this method. For brevity, the relevant details are not presented here.

The crushing strength f'_{cu} is set to zero since the residual strength of concrete after crushing is negligible. The strain at the crushing strength of concrete, ϵ_{cu} , listed in Table 2, is calculated using fracture energy balance [20]:

$$\epsilon_{cu} = \epsilon_u - \frac{1.4 \rho_s f_{yh} \epsilon_{sm}}{f'_c} \quad (29)$$

where

f_{yh} = yield strength of transverse bar, and

ϵ_u = minimum crushing strain in the cover concrete of confined concrete column.

ϵ_u is chosen as -0.005 , as was recommended in other literature [21] that found the traditionally used value of -0.003 seems to be underestimated.

ρ_s = ratio of volume of transverse confining steel to that of confined concrete core:

$$\rho_s = \rho_x + \rho_y \quad (30)$$

in which

ρ_x , and ρ_y are ratio of volume of transverse confining steel to that of confined concrete core in the x , and y directions, respectively, as shown in Fig. 21. The y direction is the loading direction.

$$\rho_x = A_{sx}/sd_c \quad (31)$$

$$\rho_y = A_{sy}/sb_c \quad (32)$$

where

s = the center to center spacing of transverse reinforcement,

A_{sx} and A_{sy} are total area of transverse reinforcement within the spacing s in x ,

and y directions, respectively, as shown in Fig. 21.

b_c and d_c are core dimensions to centerlines of perimeter hoop in x , and y directions, respectively, as shown in Fig. 21.

$$\varepsilon_{sm} = 16\varepsilon_y + 0.14 \quad (33)$$

in which

ε_{sm} = steel strain at ultimate steel stress [22], and

ε_y = yielding strain of steel.

Reasonably assuming the following:

$$\varepsilon_y = \frac{f_{yh}}{E_s} \quad (34)$$

Where E_s is the elastic modulus of steel.

E_s is assumed here to be **2040000 kgf/cm² (29000 ksi)**. The parameter λ in Table 2 was estimated to be **0.1** and is set to be fixed throughout this paper. The tensile strength of concrete is important role in the shear analysis. The peak tensile strength of concrete is given by

$$f_t = \varepsilon_{cr}E_c = 0.376\sqrt{f'_c} \text{ MPa} \quad (f_t = \varepsilon_{cr}E_c = 4.56\sqrt{f'_c} \text{ psi}) \quad (35)$$

where

ε_{cr} = cracking tensile strain of concrete = **0.00008** [4].

$$E_c = 4700\sqrt{f'_c} \text{ MPa} \quad (E_c = 57000\sqrt{f'_c} \text{ psi}) \quad (36)$$

in which

E_c = elastic modulus of concrete in accordance with ACI code [23].

Another parameter E_{ts} , listed in Table 2, controls the tension softening stiffness. The material model Concrete02 in OpenSees performed linear tension softening. Therefore the parameter E_{ts} is approximated by assuming

$$E_{ts} = \frac{\varepsilon_{cr} E_c}{1 - \varepsilon_{cr}} \quad (37)$$

3.7 Hysteretic Characteristics Of Uniaxial Cyclic Truss

Model

Fig. 22 presents a very brief example to introduce the characteristics of UCTM. Herein, a reinforced concrete column specimen subjected to reverse cyclic loading [24] is adopted to perform the analysis. The height of the column is **300 cm (118.1 in.)**. The material tests provide the average compressive strength of concrete $f'_c = 265 \text{ kg/cm}^2$ ($f'_c = 3765 \text{ psi}$) and the average tensile yield strength of hoop steels $f_y = 5000 \text{ kg/cm}^2$ ($f'_c = 71053 \text{ psi}$).

Table 3 presents the four types of cross-section. First, with the sectional properties defined, the established UCTM objects were cyclically deformed using a numerical simulation, with an increasing angle of rotation, to investigate the shear capacities of the sections. It should be clarify the calculations here is to investigate the shear behavior associated with different positions of cross sections. It is not intended to calculated the total response of the RC column.

Fig. 23 to Fig. 26 shows the relationship between the shear force and the rotational

angle that was simulated by UCTM. The results reveal severe pinching because the concrete elements were under alternating tensile and compressive strain. This phenomenon explained the pinching effect in an average global sense. Fig. 23 also shows the peak values of shear. Sections A1 and B2 shown in Fig. 23 and Fig. 26 have greater shear carrying capacities than A2 and B1 shown in Fig. 24 and Fig. 25, because they were associated with smaller transverse reinforcement spacings.

The results in Fig. 23 to Fig. 26 represent the sectional shear cyclic capacities, too. The column may or may not fail by shear fracture will depend on the corresponding flexural capacity.



Chapter 4 Comparisons Of UCTM With Experiments

To verify the proposed method, the results obtained from UCTM were compared with experimental results from seven specimens presented elsewhere [24-30] as listed in Table 4. The hysteretic loops in the experiments show that all failure involved shear showed severe pinching, except for that of specimen BMR2, which failed in flexure with saturated hysteretic loops.

4.1 SY AND LY

The notable feature of the experiments that were performed on specimens SY and LY [28-30] was that the displacements in the cyclic loading tests were smaller than those revealed by the other test data. The transverse steels are steel rounded bars while the longitudinal steels are not. Fig. 30 and Fig. 31 shows the cross-sections and the corresponding comparison between the analytical and experimental results. It can be seen that the analytical results obtained by UCTM agree closely with the experimental results. Both the failure mode and the hysteretic path are accurately predicted. The UCTM automatically decided the failure mode as shear failure. Thus the total response calculated is governed by shear with severe pinching effect rather than flexure. If it is controlled by flexure, the analytical result will show saturated hysteretic loops. The traditional methods can not perform the judgment as UCTM.

4.2 N18C

Specimen N18C [26] was used to elucidate the importance of UCTM. Fig. 32 shows its cross-section and compares the experimental data to the analytical results calculated with or without UCTM incorporated into fiber element method. The results obtained

using the fiber element method without UCTM reveal a flexural response with saturated hysteretic loops. This result clearly disagrees with the observed experimental results, which revealed shear failure with severe pinching. When UCTM is applied, the analytical results are greatly improved, and are much more consistent with the experimental data.

4.3 H-19 AND F-19

Longitudinal and transverse steel bars were steel rounded bars. Fig. 33 to Fig. 34 present cross-sections of specimens H-19 and F-19 [27] and a comparison of the corresponding simulation results with the experiment. It is shown that analytical results by the combined UCTM and fiber element method match the test results very well. The most important failure mode is accurately predicted.

4.4 BMRS

The BMRS specimen was tested in NCREE [25]. Fig. 35 to Fig. 41 show the cross-section and elevation of the RC column specimen and compare each hysteretic loop from UCTM simulations with that from experiment. It is shown that the shear failure mode is accurately predicted. The analytical results reveal severe pinching that was caused by the shear-dominated fracture. Shear forces were precisely predicted and their peaks were identified. The values of stiffness determined by the analysis are also sufficiently close to the experimental values.

4.5 BMR2 (FLEXURAL FRACTURE DOMINATED)

UCTM can be employed to analyze RC columns with variable cross-sectional properties and can predict whether failure is by the shear or flexural mode. Numerical analysis of the BMR2 specimen tested in NCREE [24] will demonstrate these functions.

Among the specimens considered in this paper, BMR2 is the most complex one, as it

has four designed cross-sections, as shown in Fig. 42. The RC column is thus divided into four elements in the simulation. Each individual part may exhibit its own failure mode. However, the analytical results show that all elements failed in flexure. In Fig. 42, the hysteretic loops revealed a flexural response. Although the response of the column was dominated by flexure, which was simulated by the fiber element method, UCTM automatically simulated the elastic shear response.



Chapter 5 Predicting Failure Behavior of Reinforced Concrete Columns Subjected to Cyclic Loading

A procedure derived from UCTM was established to predict rapidly the failure mode of a reinforced concrete column in the design stage. Failure mode of an RC column can be classified as either shear or flexural failure. In general, an RC column can be assumed to be a beam-column member subjected to combined axial, flexural, and shear forces. It is difficult to predict its overall failure behavior without a priori knowledge. Thus in this paper, the shear capacity is isolated independently from the complex behavior of a column based on the concept of well known truss model. The shear capacity can be viewed as the contribution of diagonal truss of a truss model while the longitudinal truss modeled the combined axial-flexural behavior. The obtained shear capacity using the proposed method can be compared with flexural capacity obtained from pushover analysis to predict whether shear failure or flexural failure will occur during cyclic test of an RC column. Five cyclic test results were compared to the predicted analytical results. All five failure modes are successfully predicted using the proposed procedure.

5.1 Shear Capacity of an RC Column

The shear capacity of an RC column is evaluated by the total shear force in a uniaxial cyclic truss model (UCTM), as shown in Fig. 15. It can be determined from the predefined displacement field under shear using Equation (3). For a positive value of shear deformation γ , V_{CF} is the contribution of the compressive force in the concrete element CF to the total shear force, and V_{DE} is the contribution of the tensile force in the concrete element DE to the total shear force.

The UCTM comprises three types of elements, which are concrete element under compression, concrete element under tension, and transverse reinforcement. For positive γ , these are corresponding to element CF, DE, CD (EF is identical to CD and is thus omitted from the following in discussion). In general, of these elements, only elements CD or DE can reach their ultimate strength when the total shear force reaches its ultimate value during shear deformation, unless the transverse reinforcements are designed to be unreasonably strong relative to the concrete, because of either their amount or strength. The compression strut CF remains below its ultimate strength. Notably, in practice, element CF may in fact reach its ultimate strength, and the crushing of element CF is often observed - but normally at the time of collapse of the RC column. When collapse occurs, elements CD and DE have already far exceeded their ultimate strengths. Thus, the ultimate state of element CF can be ignored, and element CF simply serves to balance force. To eliminate the need for a cyclic analysis, the strengths of elements CD and DE are assumed to be the yield strength of hoops f_{yh} and the peak tensile strength of concrete f_{tc} , respectively. If ties are present, their ultimate strength is also assumed to be f_{yh} for convenience. f_{tc} can be evaluated as

$$f_{tc} = \varepsilon_{cr} E_{cc} = \mathbf{0.376} \sqrt{f'_{cc}} \text{ MPa} \quad (f_{tc} = \varepsilon_{cr} E_{cc} = \mathbf{4.56} \sqrt{f'_{cc}} \text{ psi}) \quad (38)$$

where

ε_{cr} = cracking tensile strain of concrete = **0.00008** [4], and

$$E_{cc} = \mathbf{4700} \sqrt{f'_{cc}} \text{ MPa} \quad (E_{cc} = \mathbf{57000} \sqrt{f'_{cc}} \text{ psi}) \quad (39)$$

where

E_{cc} = elastic modulus of core concrete in accordance with ACI code [23], and

f'_{cc} = strength of core concrete [19].

The original concrete strength f'_c is replaced by the strength of the core concrete f'_{cc} , which was evaluated using a theoretical stress-strain model for confined concrete [19]. The model considers the confinement effects of surrounding longitudinal and transverse reinforcement. The horizontal force equilibrium at point C in Fig. 15 gives

$$-V_{CF} = V_{DE} + V_{CD} \quad (40)$$

where

V_{CD} = horizontal component of internal axial force in element CD.

Substituting Equation (40) into Equation (3) yields,

$$V = 2V_{DE} + V_{CD} \quad (41)$$

Equation (41) eliminates the unknown value V_{CF} . The remaining values, V_{DE} and V_{CD} , are easily calculated. The calculation of V_{DE} is intuitive. V_{DE} equals to the shear component of the internal axial force in element DE, which is the product of the concrete tensile stress and the area for element DE. The area is the total projected area of concrete element DE, as discussed earlier, in the direction parallel to transverse steel element CD.

$$V_{DE} = f_{tc} b_c d_c \sin \alpha \cos \alpha \quad (42)$$

where

b_c and d_c are core dimensions to centerlines of perimeter hoop in x and y direction, respectively, as shown in Fig. 15, and

Similarly, V_{CD} equals to the product of the yielding stress and the area of element CD.

$$V_{CD} = f_{yh} \rho_y b_c d_c \tan \alpha \quad (43)$$

where

ρ_y = ratio of volume of transverse confining steel to volume of confined concrete core in the y direction as shown in Fig. 15.

Notably, the y direction is the loading direction. For $\alpha = 45^\circ$,

$$V_{DE} = f_{tc} b_c d_c / 2 = \mathbf{0.188} \sqrt{f'_{cc}} b_c d_c \text{ (MPa)} \quad (44a)$$

$$V_{DE} = f_{tc} b_c d_c / 2 = \mathbf{2.28} \sqrt{f'_{cc}} b_c d_c \text{ (psi)} \quad (44b)$$

$$V_{CD} = f_{yh} \rho_y b_c d_c = \frac{f_{yh} A_{sy} d_c}{s} \quad (45)$$

where A_{sy} denotes the total area of the transverse reinforcement within the spacing s in the y direction.

Substituting Equations (44, 45) into Equation (41) yields the total shear force,

$$V = \frac{f_{yh} A_{sy} d_c}{s} + \mathbf{0.376} \sqrt{f'_{cc}} b_c d_c = V_s + V_c \text{ (MPa)} \quad (46)$$

$$V = \frac{f_{yh} A_{sy} d_c}{s} + \mathbf{4.56} \sqrt{f'_{cc}} b_c d_c = V_s + V_c \text{ (psi)} \quad (46)$$

where

$$V_c = \mathbf{0.376} \sqrt{f'_{cc}} b_c d_c \text{ (MPa)} \quad (47a)$$

$$V_c = \mathbf{4.56} \sqrt{f'_{cc}} b_c d_c \text{ (psi)} \quad (47a)$$

and

$$V_s = \frac{f_{yh} A_{sy} d_c}{s} \quad (47b)$$

V_c and V_s are the shear force contributed by the concrete and the transverse reinforcement, respectively. Equation (46) can be used to estimate nominal shear strength, which is similar to those recommended in ACI 318-05 [1]:

$$V_s = \frac{f_{yh} A_{sy} d}{s} \quad (48a)$$

and

$$V_c = 0.167 \sqrt{f'_c} b d \text{ (MPa)} \quad (48b)$$

$$V_c = 2 \sqrt{f'_c} b d \text{ (psi)} \quad (48b)$$

except that in which b and d in ACI 318-05 denote width and depth of the column.

The major difference between Equation (11) and Equation (12) is that f'_c has been adjusted to f'_{cc} herein. The coefficient 0.376 (4.56 in psi), derived from the tensile strength of concrete, is larger than 0.167 (2 in psi) proposed in ACI 318-05 [1]. Research [11] also indicated that the equation of nominal shear strength that was proposed in ACI 318-05 [1] severely underestimated the shear capacities of RC columns.

5.2 Flexural Capacity

The peak lateral force determined from a pushover curve generated using fiber element method without UCTM is taken to estimate the flexural resistance. Sectional properties are listed in Table 5. f'_{cc} are accordingly calculated.

5.3 Failure Mode Prediction

The nominal shear strengths and peak lateral forces of all specimens in this study are calculated using the proposed method. Table 6 and Table 7 lists the results. Conceptually, shear and flexural models can be considered as springs that are connected in series to determine the relationship between lateral force and deformation. Since the simplified method was derived using this method, the smaller one between the nominal shear strength and peak lateral force will reasonably determine the failure mode. Table 6 and

Table 7 compared the predicted failure modes with those revealed by experiments. Even for specimens SY and LY, the nominal shear strength and peak lateral force were very close to each other, all of the predicted failure modes are consistent with the test results.



Chapter 6 Conclusions

Based on the results of this paper, the following conclusions are drawn:

1. The proposed UCTM (Uniaxial Cyclic Truss Model) is a vessel to produce a uniaxial shear model. The complex multiaxial shear behavior is condensed into uniaxial model in our research.
2. UCTM provides a method to determine the uniaxial hysteretic relationship between the shear forces and shear rotational angle. Sectional and material properties are reduced to five realistic parameters with simple physical meanings. From these basic parameters, UCTM determines shear force and shear stiffness for given shear deformation. No additional regression technique is required to perform the analysis.
3. Comparing with experimental results, the overall results based on UCTM are quite well. If the cross-section of an RC column is given, the total response of the column can be determined, regardless of whether it fails in flexural or shear mode.
4. Most literatures could not clearly identify the difference between shear failure mode and flexural failure mode. Most of the shear model in literatures could not possess the trend of cyclic shear response of an RC column. The model we established can identify clearly the difference without basing on any assumption which many other models in other literatures have to.
5. Most analytical methods simulating the shear response of an RC column require the *a priori* assumption that the RC columns will fail in shear. If the failure mode cannot be known in prior, then such methods fail. UCTM, combining with flexural analysis method, does not suffer from this problem. Since UCTM and the flexural analysis method are connected as springs in series to determine the relationship

between lateral force and deformation, the overall model can identify the failure mode and simulate it.

6. The method for simulating the flexural response can be easily changed by object-oriented programming if required. The concrete and steel material models in UCTM can be replaced with preferred material models. So that one of the merit of UCTM is its flexibility.
7. The proposed simplified method combining with pushover method can identify the failure mode easily. The complex shear behavior of an RC column is simplified into an elegant procedure. The shear capacity can be calculated even without a computer. Failure modes of specimens from different laboratories in different locations are all successfully predicted using the proposed method.
8. UCTM uses ReinforcingSteel object as transverse steel model as shown in Fig. 20. This steel model is designed to be used as longitudinal steels. It sustained no strength degradation. So is the UCTM. The envelope of the hysteretic model associated with UCTM is determined by the steel model. It can be considered to develop a more realistic transverse steel model in the future. It means the hoops and ties should sustained to strength and stiffness degradation seriously. Once such model was used in UCTM, the associated hysteretic model should sustained to severe strength and stiffness degradation.

REFERENCE



- [1] *Building code requirements for structural concrete (ACI 318-05) and commentary (ACI 318R-05)*. Farmington Hills, Mich.: American Concrete Institute, 2005.
- [2] F. J. Vecchio and M. P. Collins, "Modified compression-field theory for reinforced concrete elements subjected to shear," *Journal of the American Concrete Institute*, vol. 83, pp. 219-231, 1986.
- [3] M. P. Collins and D. Mitchell, *Prestressed concrete structures*. Englewood Cliffs, N.J.: Prentice Hall, 1991.
- [4] T. T. C. Hsu and R. R. H. Zhu, "Softened membrane model for reinforced concrete elements in shear," *ACI Structural Journal*, vol. 99, pp. 460-469, 2002.
- [5] R. R. H. Zhu and T. T. C. Hsu, "Poisson effect in reinforced concrete membrane elements," *ACI Structural Journal*, vol. 99, pp. 631-640, 2002.
- [6] M. Mansour and T. T. C. Hsu, "Behavior of reinforced concrete elements under cyclic shear. II: Theoretical model," *Journal of Structural Engineering*, vol. 131, pp. 54-65, 2005.
- [7] Y. L. Mo, "Analysis and design of low-rise structural walls under dynamically applied shear forces," *ACI Structural Journal*, vol. 85, pp. 180-189, 1988.
- [8] G. Ozcebe and M. Saatcioglu, "Hysteretic shear model for reinforced concrete members," *Journal of structural engineering*, vol. 115, pp. 132-148, 1989.
- [9] W. Ritter, "Die bauweise hennebique," *Schweizerische Bauzeitung*, vol. 33, pp. 59-61, 1899.
- [10] E. Mörsch, *Der eisenbetonbau: seine theorie und anwendung*. Stuttgart: Verlag Konrad Wittner, 1912.
- [11] C. L. Wu, S. J. Hwang, Y. S. Yang, and R. S. Su, "Shake Table Tests on Reinforced Concrete Short Columns Failing in Shear," National Center for Research on Earthquake Engineering, Taiwan NCREE-07-033, 2007.
- [12] A. H. Nilson, D. Darwin, and C. W. Dolan, *Design of concrete structures*, 13th ed.: McGraw Hill, 2003.
- [13] F. Taucer, E. Spacone, F. C. Filippou, B. E. E. R. C. University of California, T. California. Dept. of, and F. National Science, *A fiber beam-column element for seismic response analysis of reinforced concrete structures*. Berkeley, Calif.: Earthquake Engineering Research Center, College of Engineering, University of California, 1991.
- [14] F. McKenna, G. L. Fenves, and M. H. Scott. (2004, 4/29). *OpenSees: open system for earthquake engineering simulation*. Available: <http://opensees.berkeley.edu>
- [15] R. D. Cook, *Concepts and applications of finite element analysis*, 4th ed. New York: Wiley, 2002.
- [16] J. H. Kim, J. B. Mander, and Multidisciplinary Center for Earthquake Engineering Research (U.S.), *Truss modeling of reinforced concrete shear-flexure behavior*. Buffalo, N.Y.: Multidisciplinary Center for Earthquake Engineering Research, 1999.
- [17] S. Mazzoni, F. McKenna, M. H. Scott, G. L. Fenves, and e. al. (2006, 4/29). *OpenSees users manual version 2.0*.
- [18] B. B. Welch, K. Jones, and J. Hobbs, *Practical programming in Tcl/Tk*, 4th ed. Upper Saddle River, NJ: Prentice Hall, 2003.

- [19] J. B. Mander, M. J. N. Priestley, and R. Park, "Theoretical stress-strain model for confined concrete," *Journal of structural engineering*, vol. 114, pp. 1804-1826, 1988.
- [20] T. Paulay and M. J. N. Priestley, *Seismic design of reinforced concrete and masonry buildings*. New York: Wiley, 1992.
- [21] R. Park, M. J. N. Priestley, and W. D. Gill, "Ductility of square-confined concrete columns," vol. 108, pp. 929-950, 1982.
- [22] D. C. Kent and R. Park, "Flexural Members with Confined Concrete," *Journal of the Structural Division*, vol. 91, pp. 1969-1990, July 1971.
- [23] J. C. McCormac and J. K. Nelson, *Design of reinforced concrete*, 7th ed. Hoboken, NJ: John Wiley, 2006.
- [24] K. C. Chang and H. F. Chang, "Seismic analysis of reinforced concrete columns of bridge and research about retrofit of FRP," National Center for Research on Earthquake Engineering, Taiwan 1999.
- [25] K. C. Chang and F. S. Chung, "Seismic retrofit study of RC columns lap-spliced at plastic hinge zone," National Center for Research on Earthquake Engineering, Taiwan 2000.
- [26] Y. Ryu, T. Nakamura, and M. Yoshimura, Eds., *RC column's loss of axial load carrying capacity* (Summaries of Technical Papers of Annual Meeting. Japan: Architectural Institute of Japan, 2001, p.^pp. Pages.
- [27] M. Jun, M. Bunno, K. Nagayama, M. Maeda, A. Tasai, and M. Nagata, Eds., *An evaluation of residual seismic capacity of reinforced concrete buildings base on the damage of columns part 1. outline of the test and results* (Summaries of Technical Papers of Annual Meeting. Architectural Institute of Japan, 2001, p.^pp. Pages.
- [28] K. Nitta, M. Hirabayashi, N. Hanai, H. Umemura, and T. Ichinose, Eds., *Size effect on strength deterioration of RC members (part1: outline of experiment)* (Summaries of Technical Papers of Annual Meeting. Architectural Institute of Japan, 2005, p.^pp. Pages.
- [29] M. Hirabayashi, K. Nishimura, N. Hanai, T. Ichinose, and H. Umemura, Eds., *The influence of loading history and reinforcement on strength deterioration of RC members (part1: outline of experiment)* (Summaries of Technical Papers of Annual Meeting. Architectural Institute of Japan, 2004, p.^pp. Pages.
- [30] M. Hirabayashi, K. Nitta, N. Hanai, H. Umemura, and T. Ichinose, Eds., *Size effect on strength deterioration of RC members (part2: results in normal-strength specimens)* (Summaries of Technical Papers of Annual Meeting. Architectural Institute of Japan, 2005, p.^pp. Pages.

TABLES AND FIGURES

Table 1–Assumed input parameters of “ReinforcingSteel” material

Label	Description	Assumed value
f_{yh}	yield stress in tension *	Test value
f_u	ultimate stress in tension	$1.5f_{yh}$
E_s	initial elastic tangent	2040000 kgf/cm² (29000 ksi)
E_{sh}	tangent at initial strain hardening	0.02E_s
ϵ_{sh}	strain corresponding to initial strain hardening	8ε_y
ϵ_u	strain at peak stress	$\epsilon_y + (f_u - f_{yh}) / 0.01E_s$
*This is the only one material parameter that must be determined by testing: the rest can be calculated or estimated.		



Table 2–Assumed input parameters of “Concrete02” material

Label	Description	Assumed value
f'_c	compressive strength*	Cover concrete: Test value Core concrete: Adjusted value [19]
ε_{co}	strain at compressive strength	Calculated value [19]
f'_{cu}	crushing strength	0
ε_{cu}	strain at crushing strength	Equation (29)
λ	ratio between unloading slope at ε_u and initial slope	0.1
f_t	tensile strength	Equation (35)
E_{ts}	tension softening stiffness	Equation (37)
*This is the only one material parameter that must be determined by testing: the rest can be calculated or estimated.		

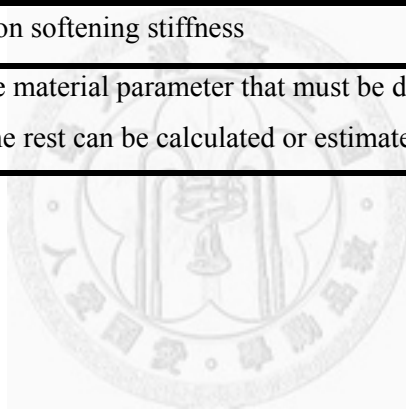


Table 3–Properties of cross-sections of the RC column

Number	Location, cm (in.)	Section	Transverse reinforcement spacing, cm (in.)
A1	0-78 (0-30.7)	A	13 (5.1)
A2	78-180 (30.7-70.9)	A	24 (9.4)
B1	180-222 (70.9-87.4)	B	24 (9.4)
B2	222-300 (87.4-118.1)	B	13 (5.1)



Table 4—Material properties of all specimens

Specimen	Column height, cm (in.)	Axial force, kN (kips)	Boundary condition on top of the column	Compressive strength of concrete, kg/cm ² (psi)	Yield strength of longitudinal steel bars, kg/cm ² (psi)	Yield strength of hoops, kg/cm ² (psi)	Yield strength of ties, kg/cm ² (psi)	Reference
BMRS	150 (59.1)	1391 (312)	Free	170 (2416)	4300 (61105)	4200 (59684)	—	[25]
BMR2	300 (118.1)	927 (208)	Free	265 (3766)	3500 (49737)	5000 (71053)	5000 (71053)	[24]
N18C	90 (35.4)	429 (96)	Fixed	270 (3837)	3874 (55052)	3823 (54327)	—	[26]
H-19	75 (29.5)	243 (55)	Fixed	248 (3524)	3303 (46938)	3293 (46795)	—	[27]
F-19	150 (59.1)	976 (219)	Fixed	249 (3538)	3028 (43030)	3354 (47662)	—	[27]
SY	40 (15.7)	273 (61)	Free	300 (4263)	4077* (57937*)	5498 (78130)	—	[28-30]
LY	80 (31.4)	913 (205)	Free	272 (3865)	4076 (57922)	4515 (64161)	—	[28-30]

* In specimen SY [28], with reference to a related study [29], the yield strength of the longitudinal steel bars was estimated to be 400 N/mm² (4077 kN, 57937 psi), owing to absence of the test data in the original study [28]. This value results in minor changes of the cyclic response of an RC column under shear failure, simulated by UCTM.

Table 5–Sectional properties and calculated strength of core concrete

Specimen		A_{sx} , cm ² (in. ²)	d_c , cm (in.)	b_c , cm (in.)	s , cm (in.)	f'_{cc} , kg/cm ² (psi)
BMRS		1.43 (0.22)	55.95 (8.67)	70.95 (11.00)	30 (4.65)	182 (2586)
BMR2	0-78 cm (0-30.7 in.)	2.85 (0.44)	55.95 (8.67)	70.95 (11.00)	13 (2.02)	352 (5002)
	78-180 cm (30.7-70.9 in.)	2.85 (0.44)	55.95 (8.67)	70.95 (11.00)	24 (3.72)	321 (4562)
	180-222 cm (70.9-87.4 in.)	2.85 (0.44)	55.95 (8.67)	70.95 (11.00)	24 (3.72)	310 (4405)
	222-300 cm (87.4-118.1 in.)	2.85 (0.44)	55.95 (8.67)	70.95 (11.00)	13 (2.02)	350 (4974)
N18C		0.63 (0.10)	23.23 (3.60)	23.23 (3.60)	10 (1.55)	311 (4419)
H-19		0.57 (0.09)	15.50 (2.4)	20.50 (3.18)	15 (2.33)	260 (3695)
F-19		2.26 (0.35)	31.11 (4.82)	41.11 (6.37)	30 (4.65)	261 (3709)
SY		0.25 (0.04)	21.9 (3.39)	21.9 (3.39)	4 (0.62)	369 (5244)
LY		1.00 (0.16)	43.8 (6.79)	43.8 (6.79)	6.6 (1.02)	340 (4832)

Table 6–Failure predicted by simplified UCTM

Specimen		V_s , kN (kips)	V_c , kN (kips)	Nominal Shear Strength, kN (kips)	Peak Lateral Force, kN (kips)	Predicted Failure Mode	Experimental Failure Mode
BMRS		139 (31)	631 (142)	770 (173)	940 (211)	Shear	Shear
BMR2	0-78 cm	763 (171)	878 (197)	1641 (368)	354 (79)	Flexure	Flexure
	78-180 cm	413 (93)	837 (188)	1251 (281)		Flexure	
	180-222 cm	413 (93)	823 (185)	1236 (278)		Flexure	
	222-300 cm	763 (171)	874 (196)	1637 (368)		Flexure	



Table 7–Failure predicted by simplified UCTM

Specimen	V_s , kN (kips)	V_c , kN (kips)	Nominal Shear Strength, kN (kips)	Peak Lateral Force, kN (kips)	Predicted Failure Mode	Experimental Failure Mode
N18C	55 (12)	112 (25)	167 (37)	340 (76)	Shear	Shear
H-19	25 (6)	60 (13)	85 (19)	132 (30)	Shear	Shear
F-19	102 (23)	243 (55)	345 (77)	541 (121)	Shear	Shear
SY	74 (17)	109 (24)	183 (41)	195 (44)	Shear	Shear
LY	295 (66)	417 (94)	712 (160)	754 (169)	Shear	Shear



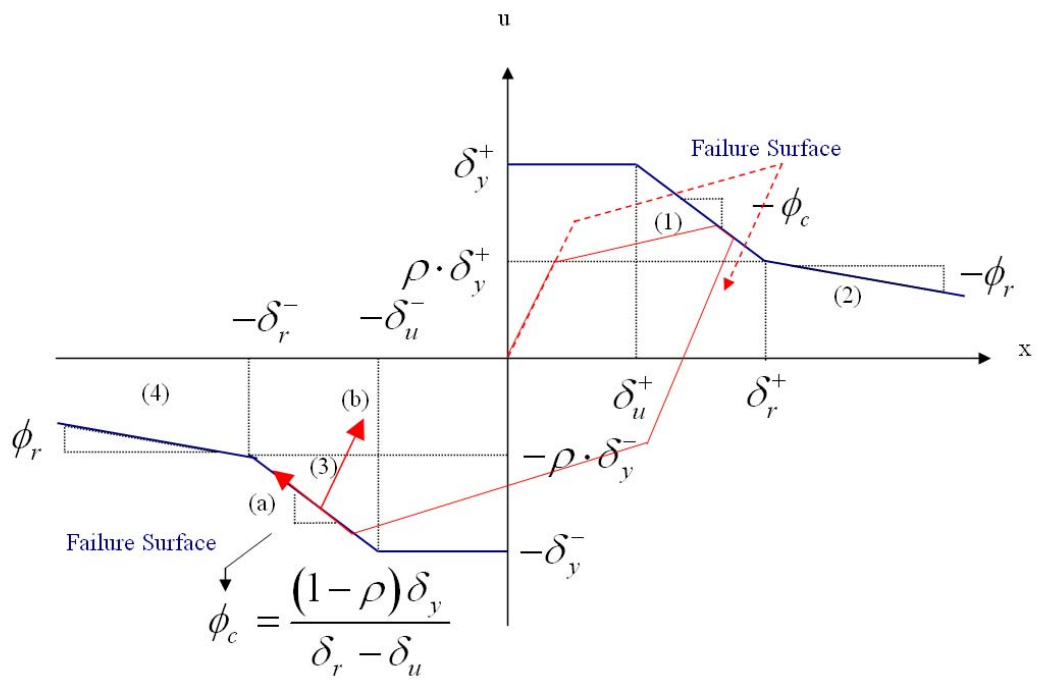


Fig. 1–A parametric model simulating failure behavior of an RC column



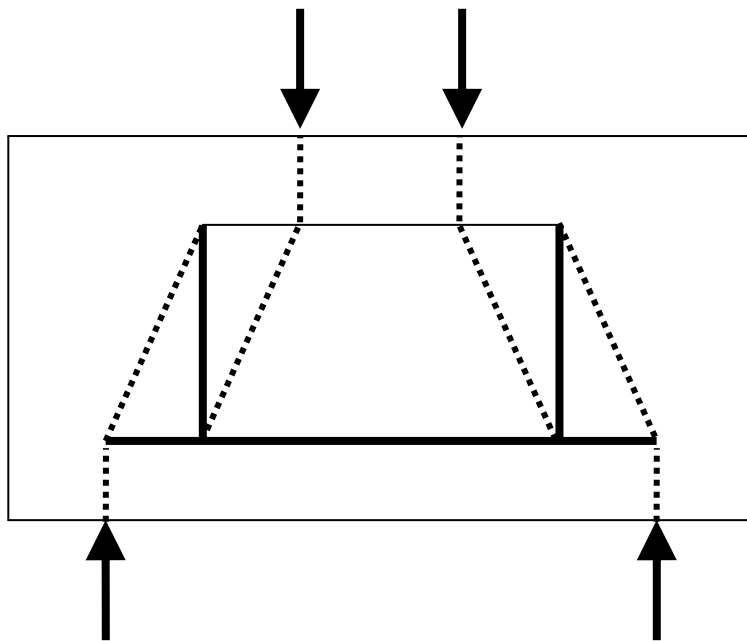
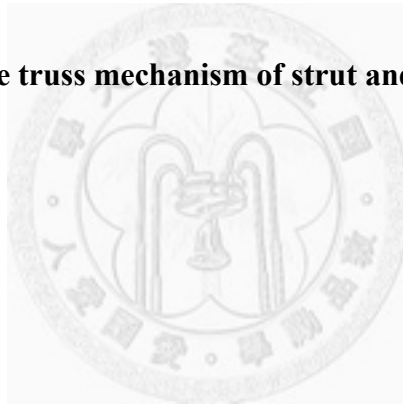


Fig. 2—The truss mechanism of strut and tie model



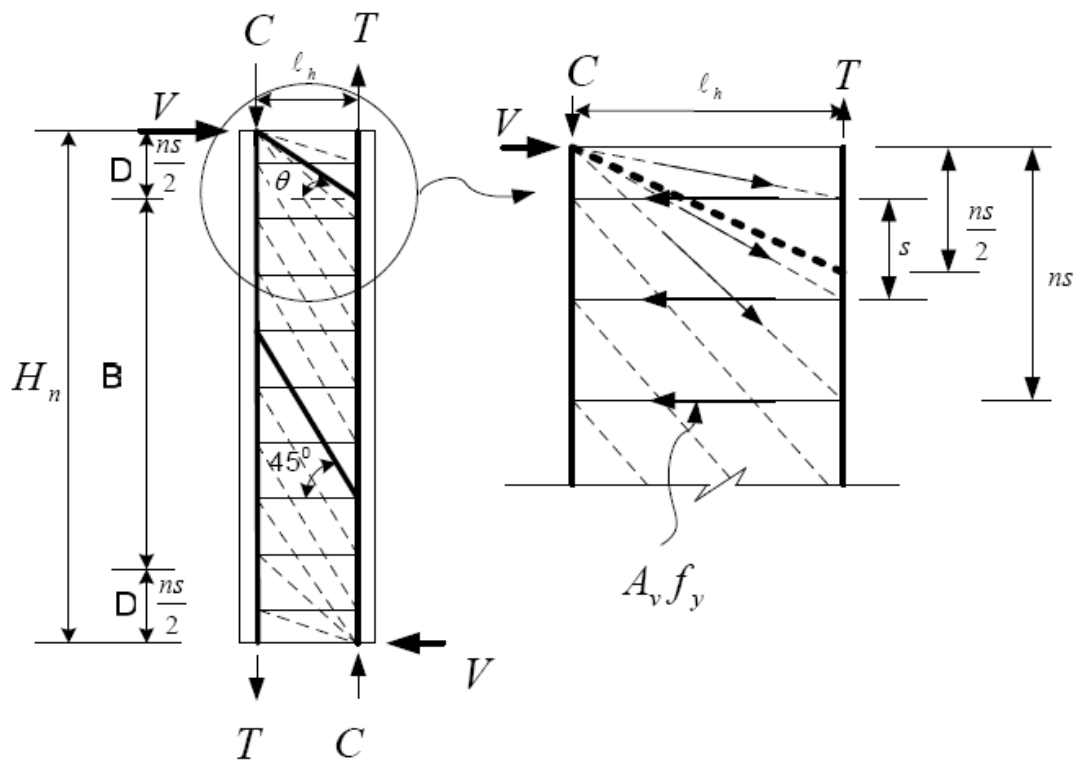
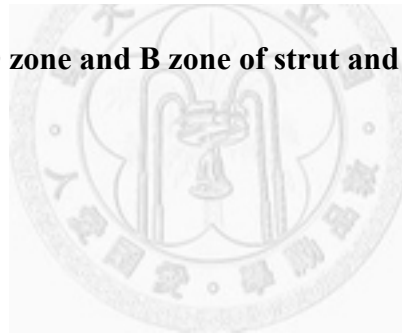


Fig. 3-D zone and B zone of strut and tie model



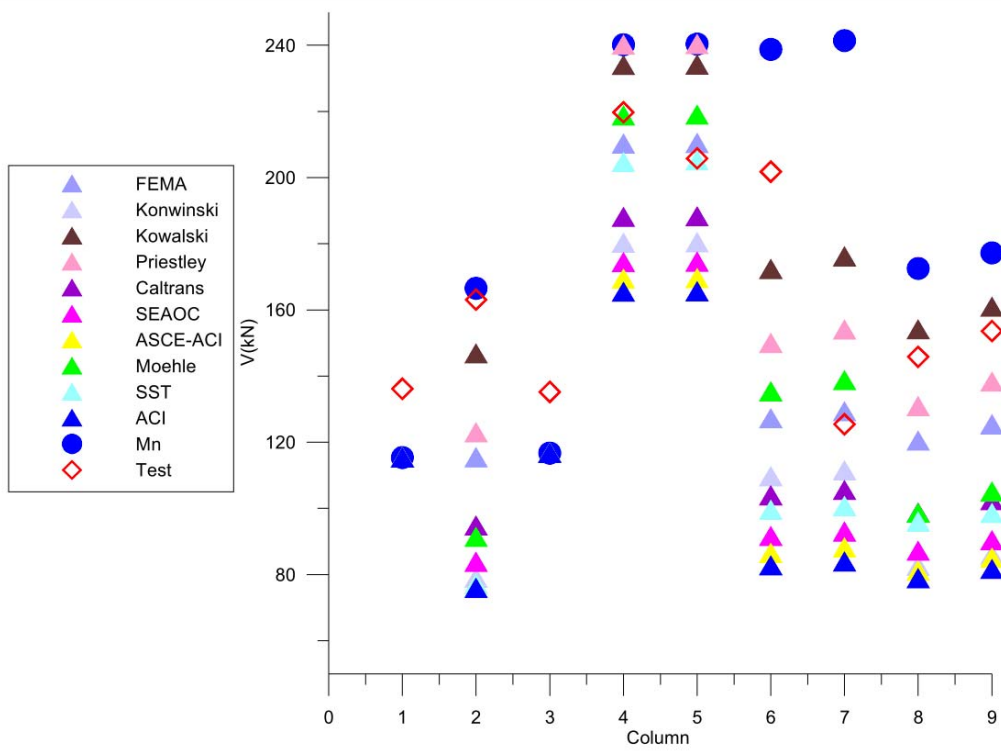


Fig. 4—Comparison of analytical and experimental shear strength



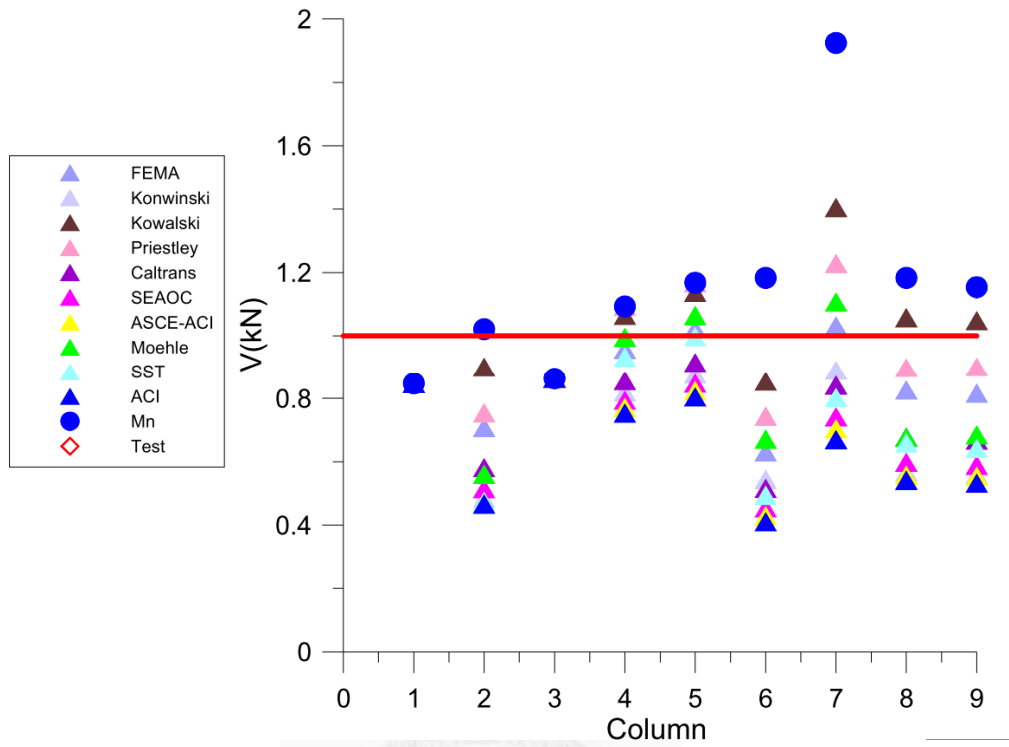
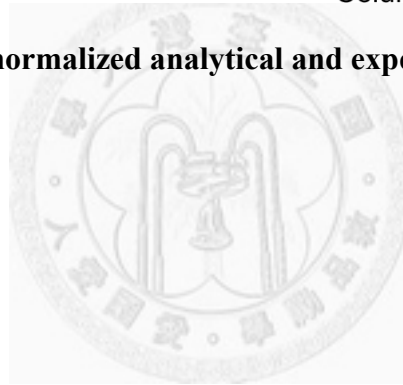


Fig. 5–Comparison of normalized analytical and experimental shear strength



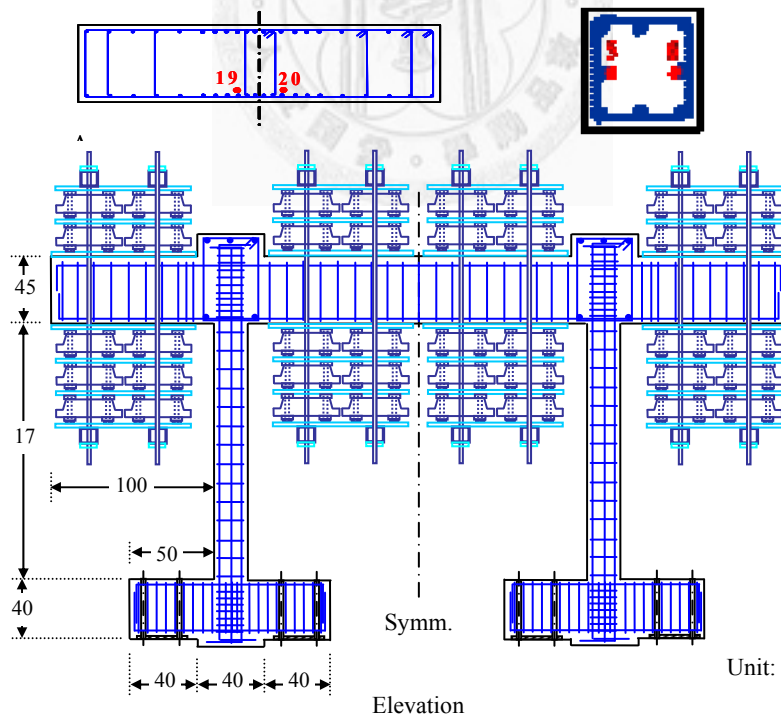


Fig. 6–Lateral View of experimental configuration of a shaking table test specimen.

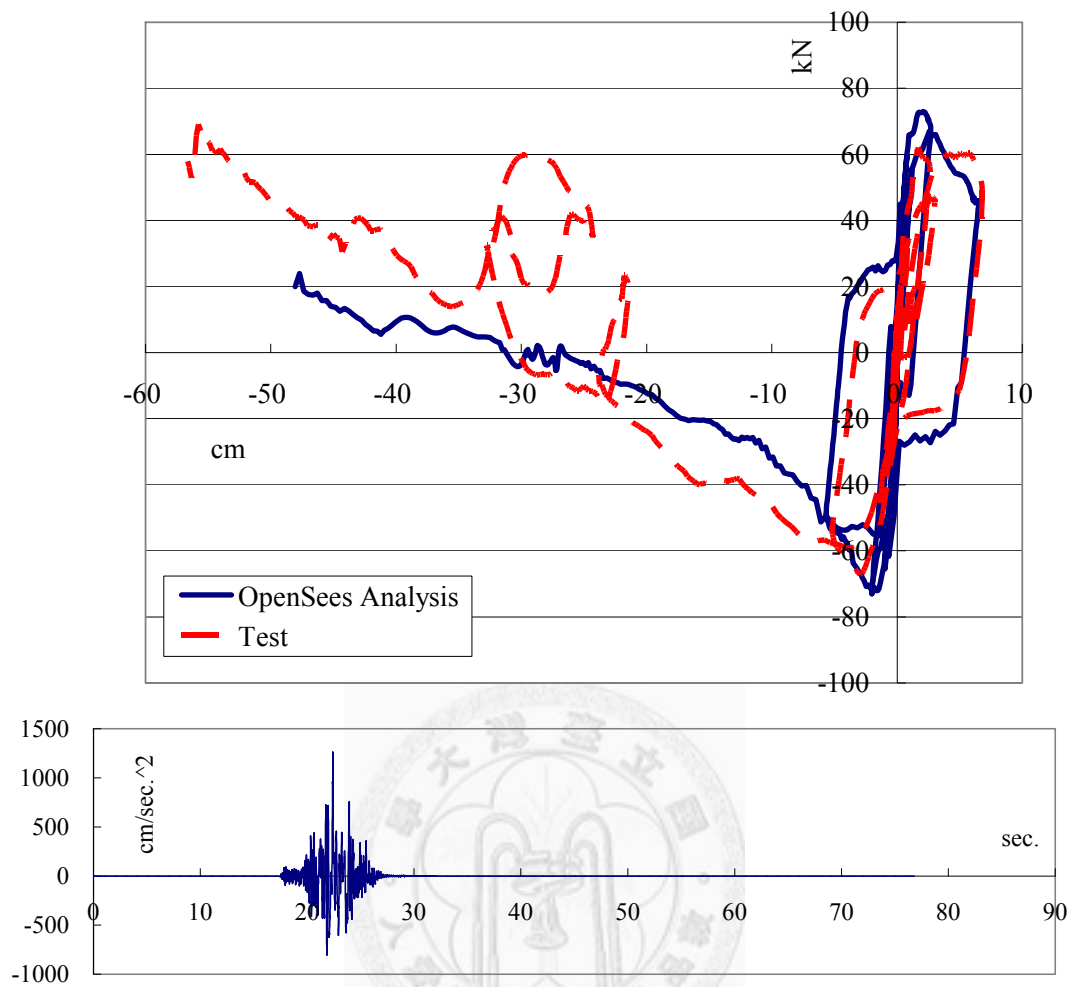


Fig. 7–Analytical prediction of relationship between lateral force and displacement of a shaking table test specimen

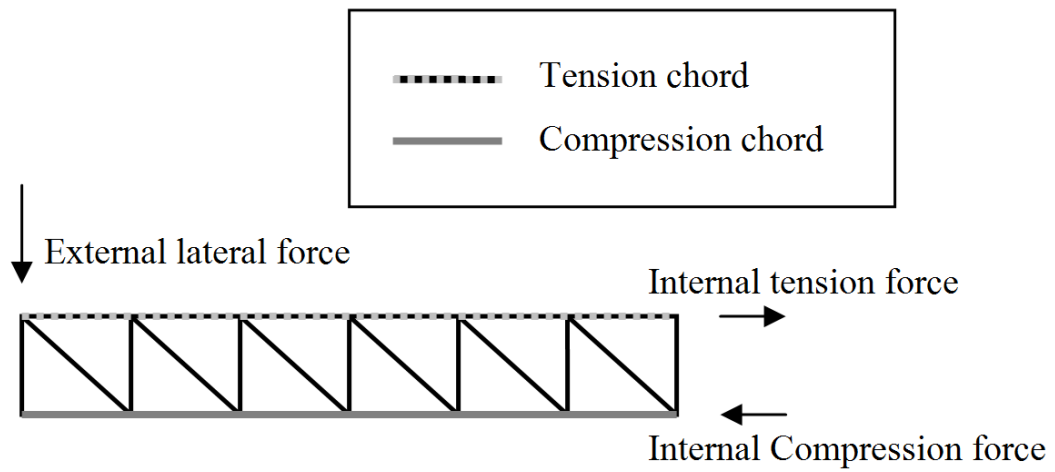


Fig. 8–Truss model of a cantilever beam subjected to lateral force.



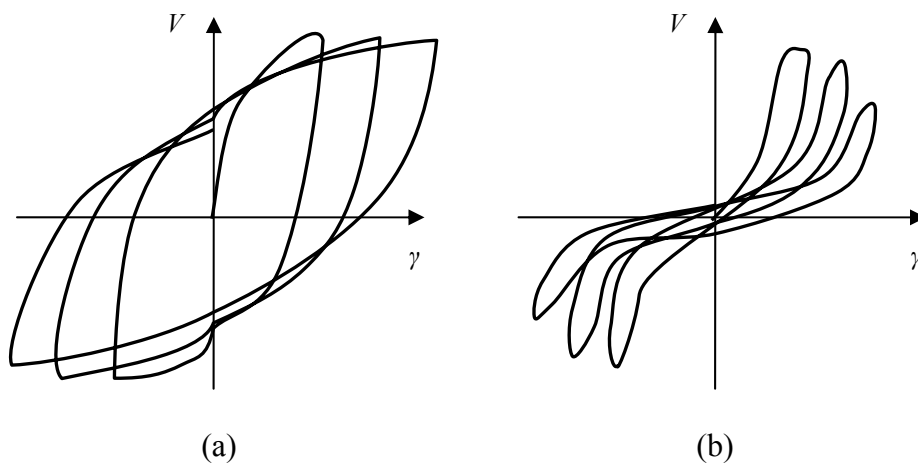


Fig. 9–Typical fracture mode of RC column in cyclic test:

(a) Flexural failure (b) Shear failure.



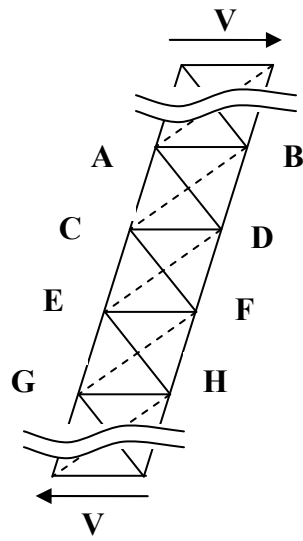


Fig. 10–RC column subjected to lateral force on top and bottom.



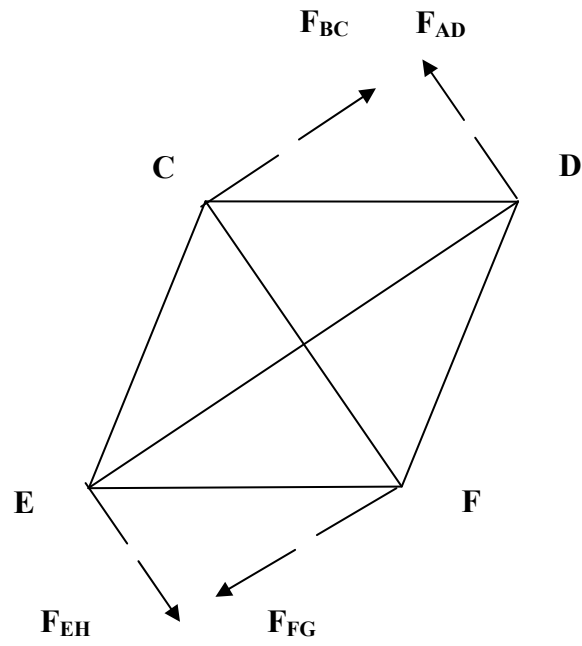


Fig. 11–Equilibrium diagrams of internal forces in UCTM (undeformed).



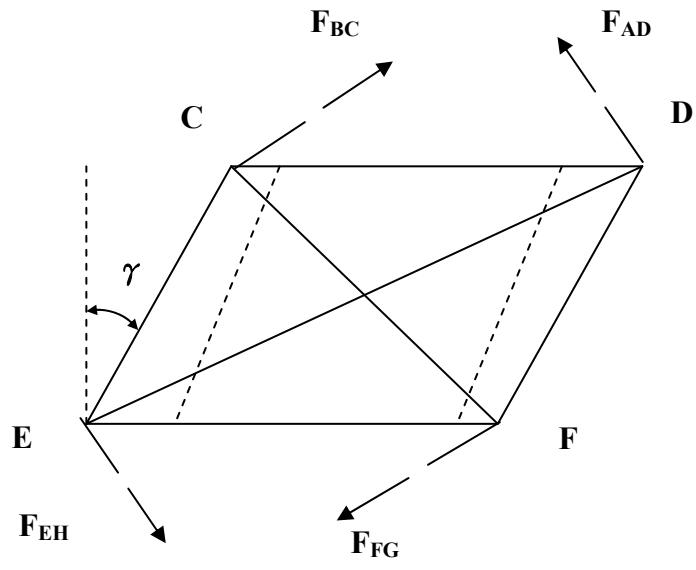


Fig. 12–Equilibrium diagrams of internal forces in UCTM (deformed).



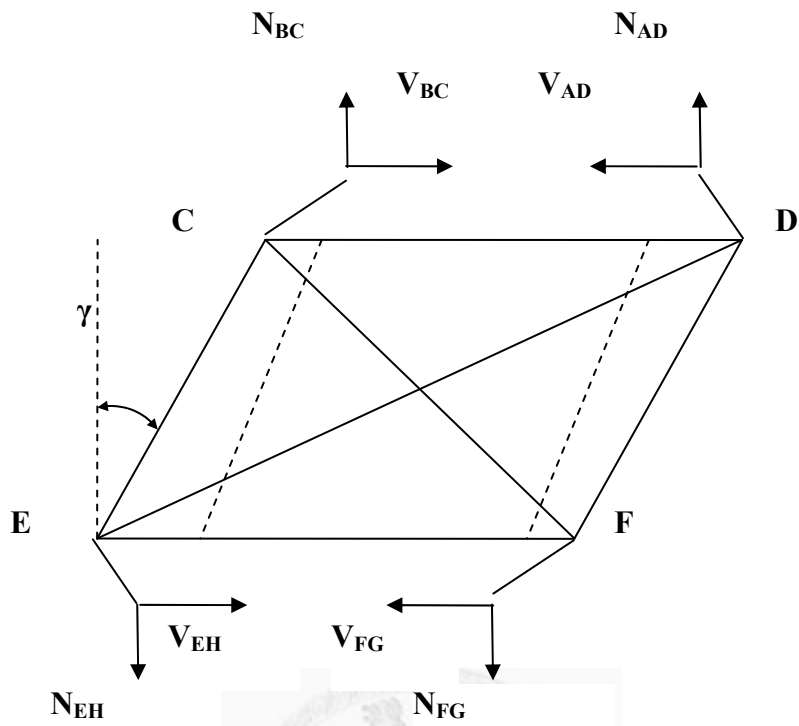


Fig. 13—Components of internal forces in UCTM.

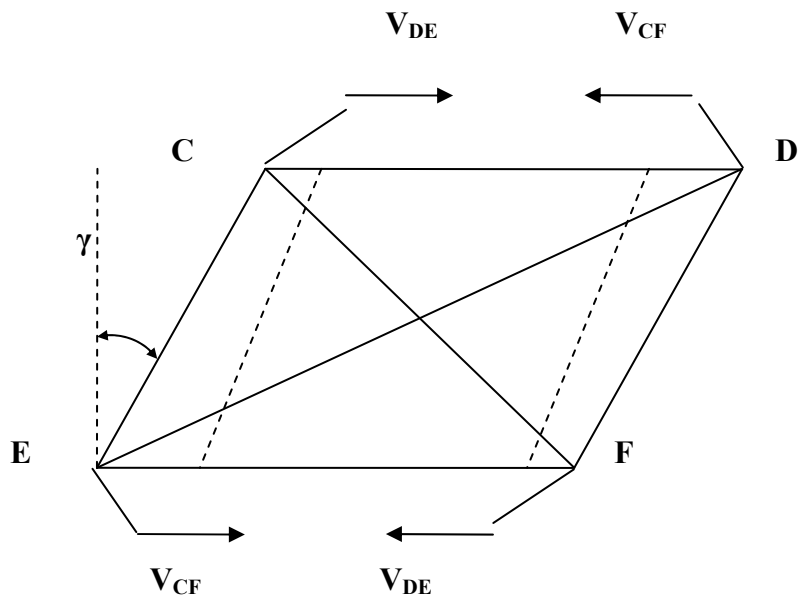


Fig. 14–Equilibrium diagrams of shear forces in UCTM.



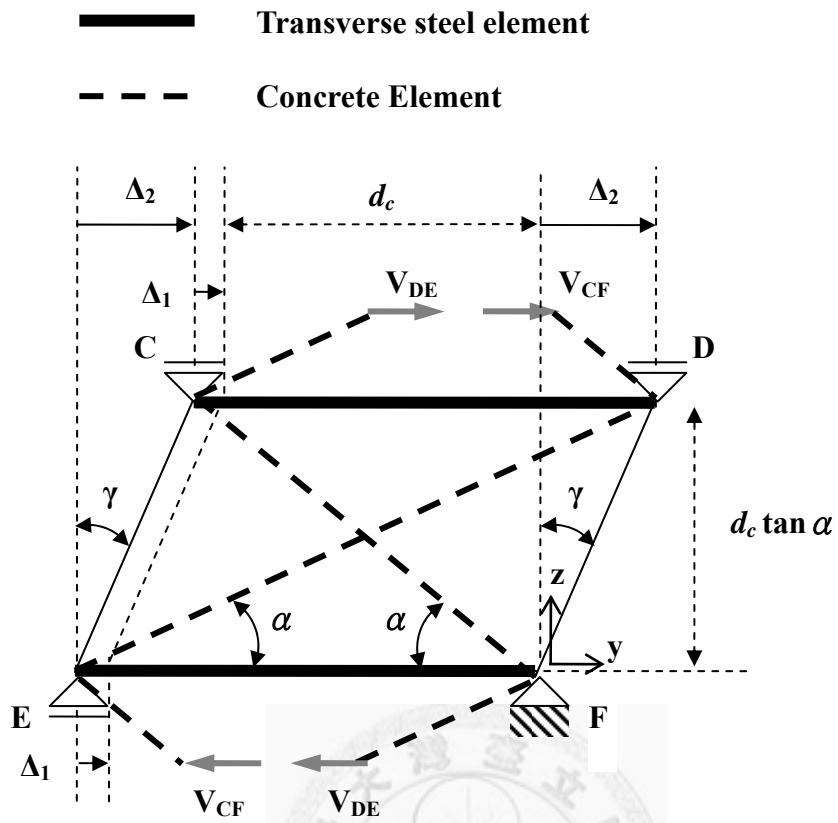


Fig. 15–Uniaxial cyclic truss model (UCTM).

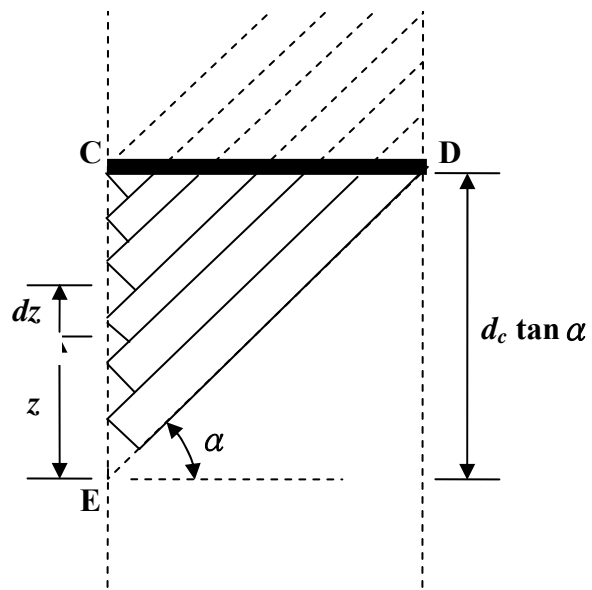
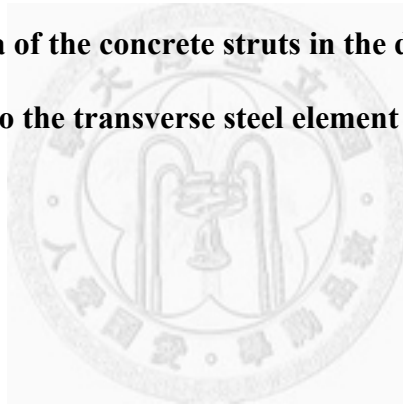


Fig. 16–Projected area of the concrete struts in the direction parallel to DE onto the transverse steel element CD.



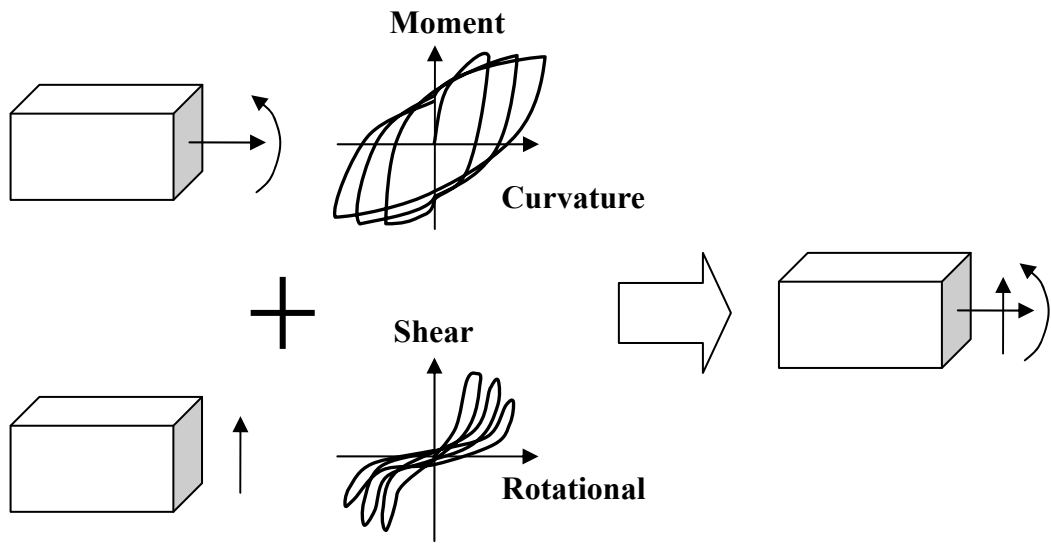
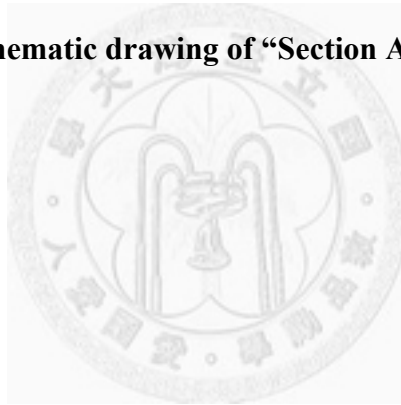


Fig. 17–Schematic drawing of “Section Aggregator”.



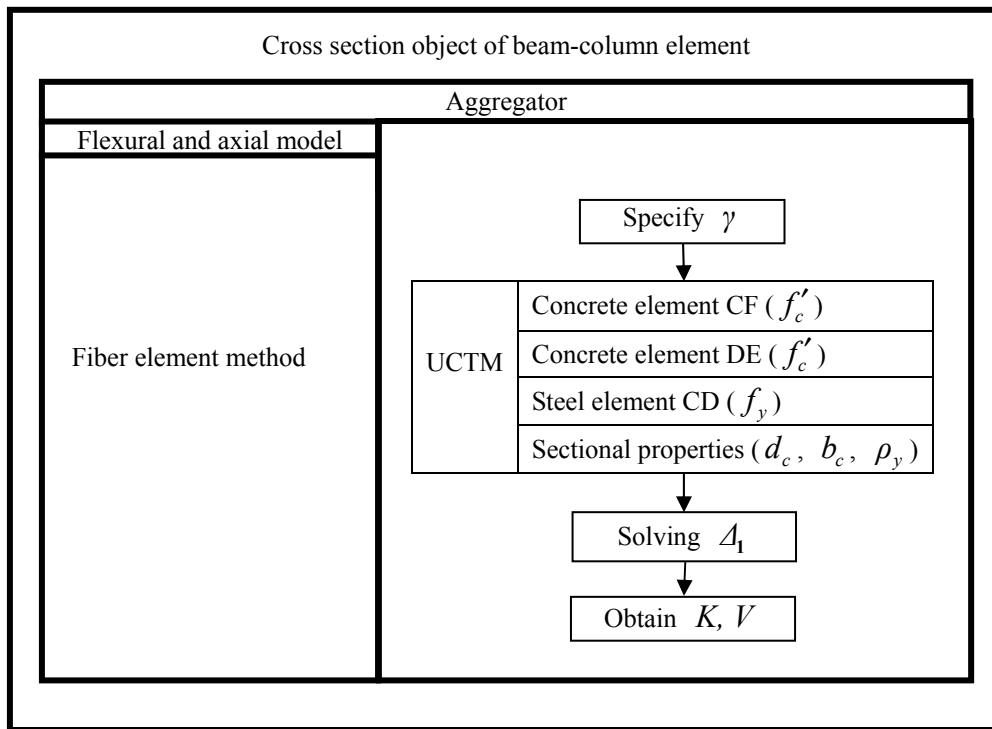
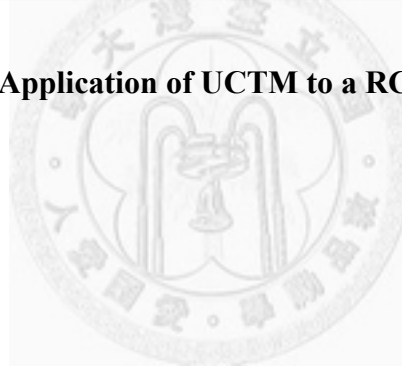


Fig. 18–Application of UCTM to a RC column.



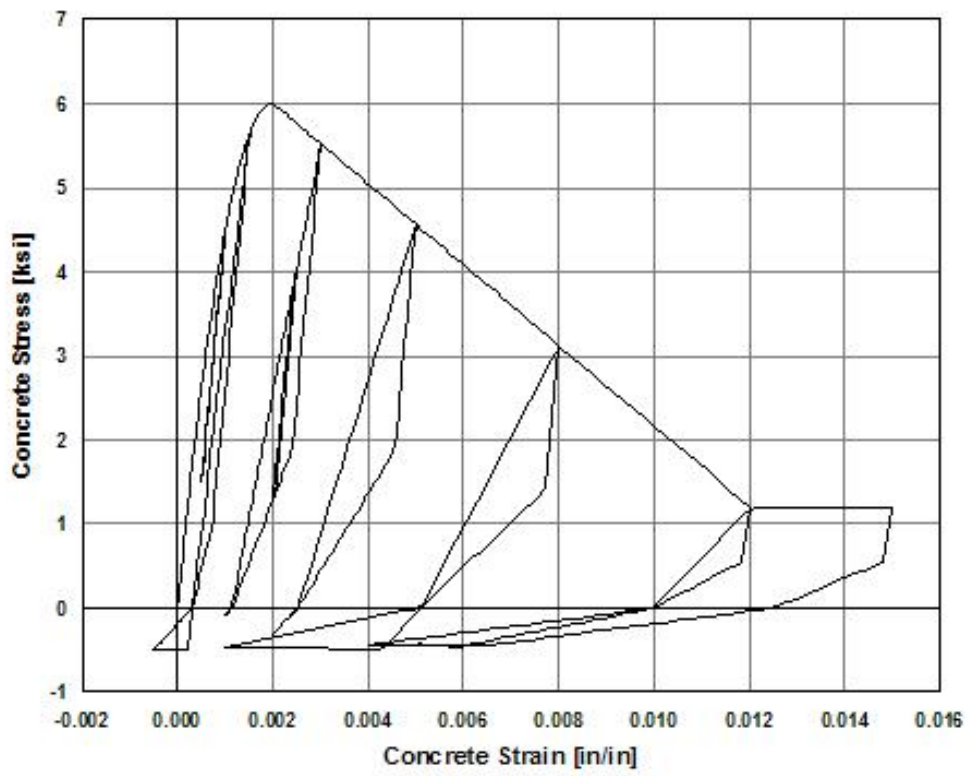
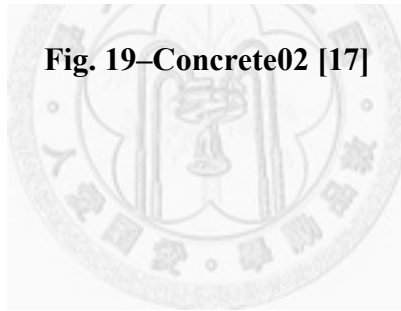


Fig. 19–Concrete02 [17]



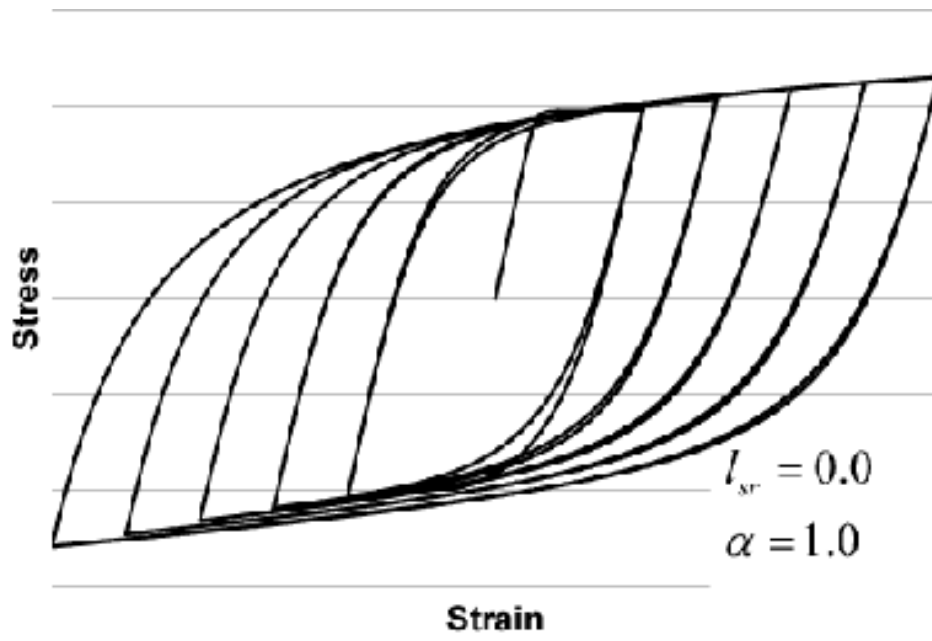


Fig. 20–ReinforcingSteel [17]



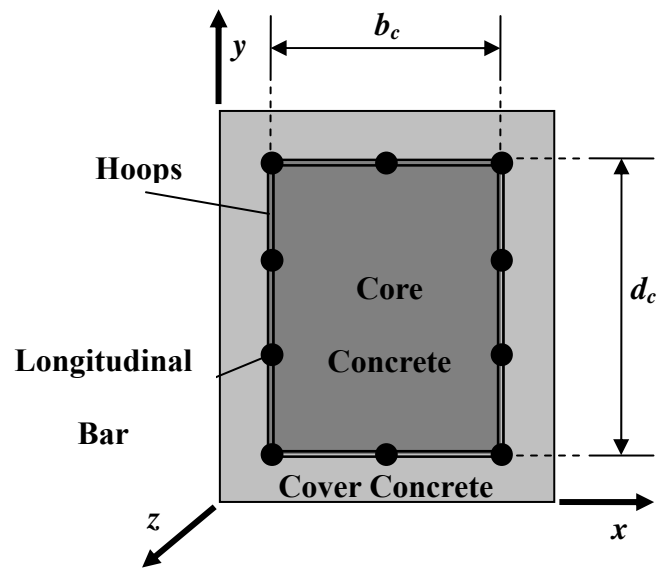
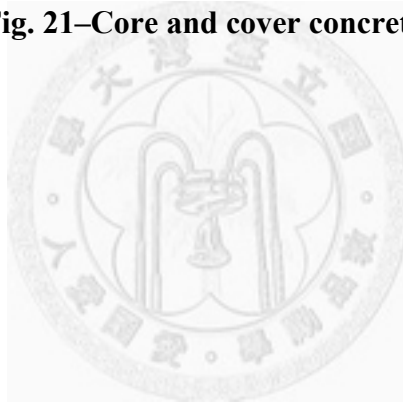


Fig. 21–Core and cover concrete.



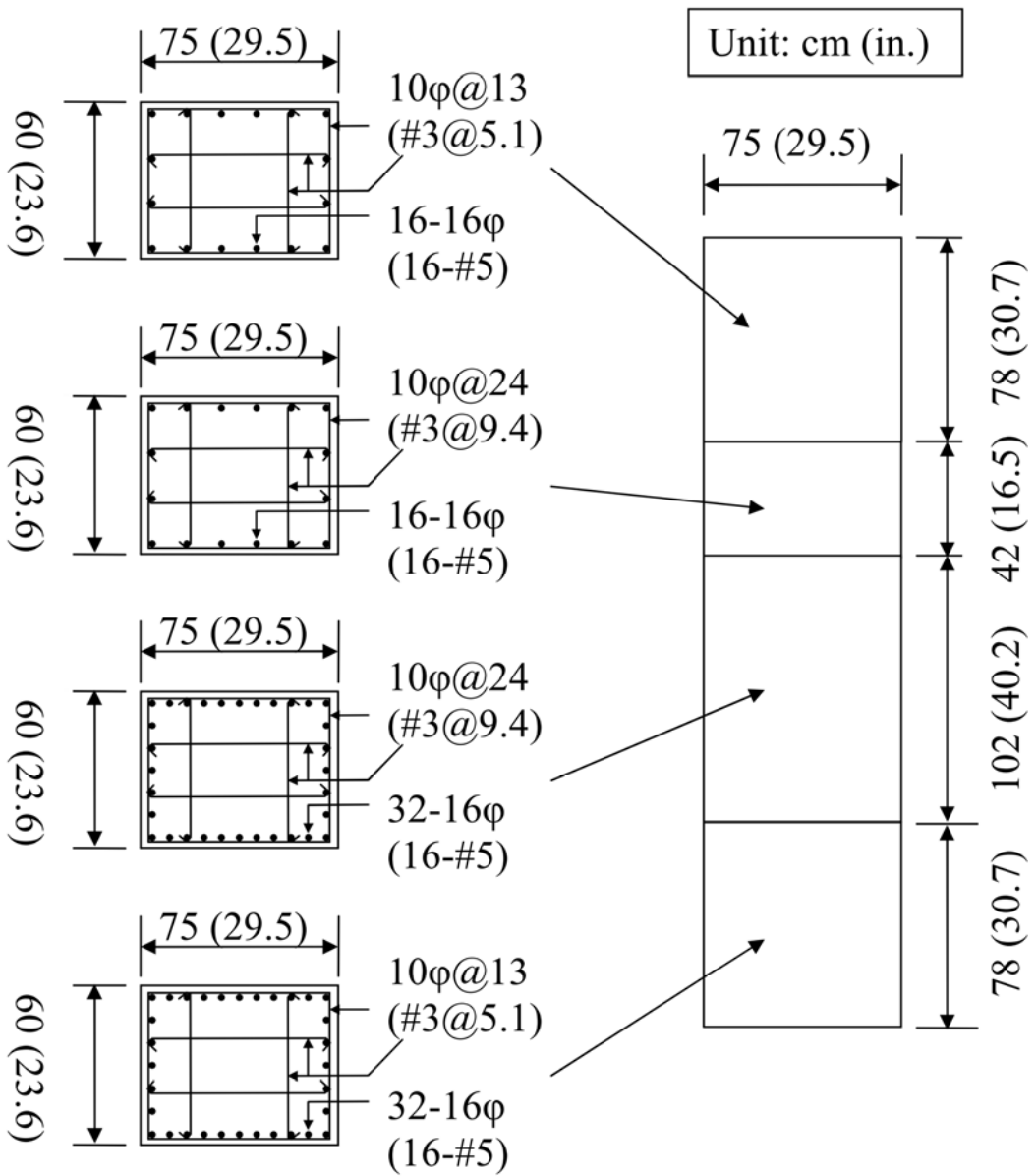


Fig. 22–Lateral view of experimental configuration.

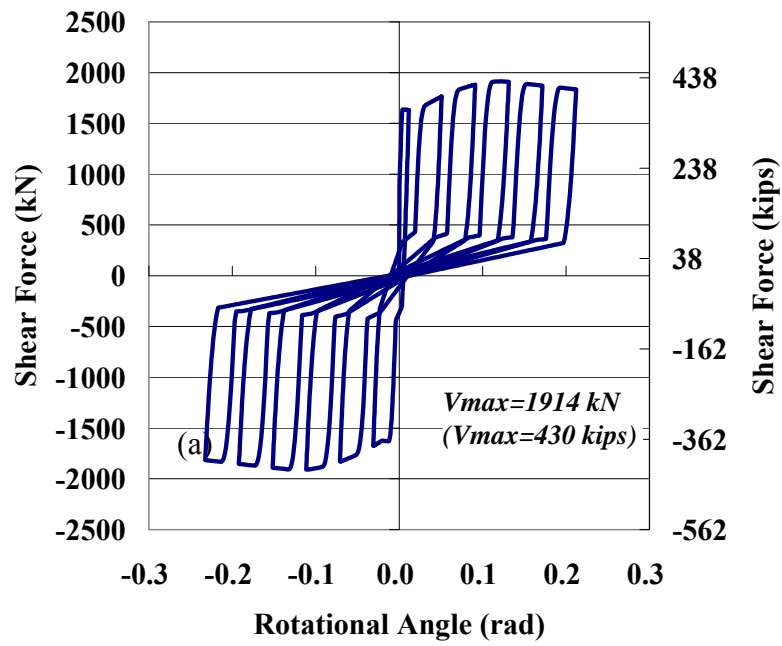
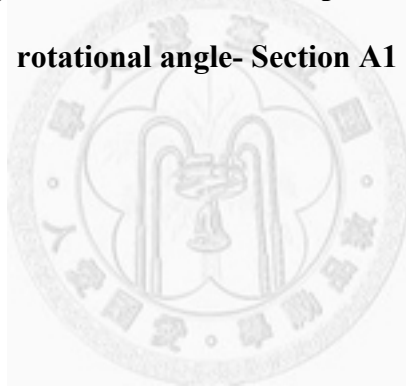


Fig. 23—Analytical prediction of relationship between shear force and rotational angle- Section A1



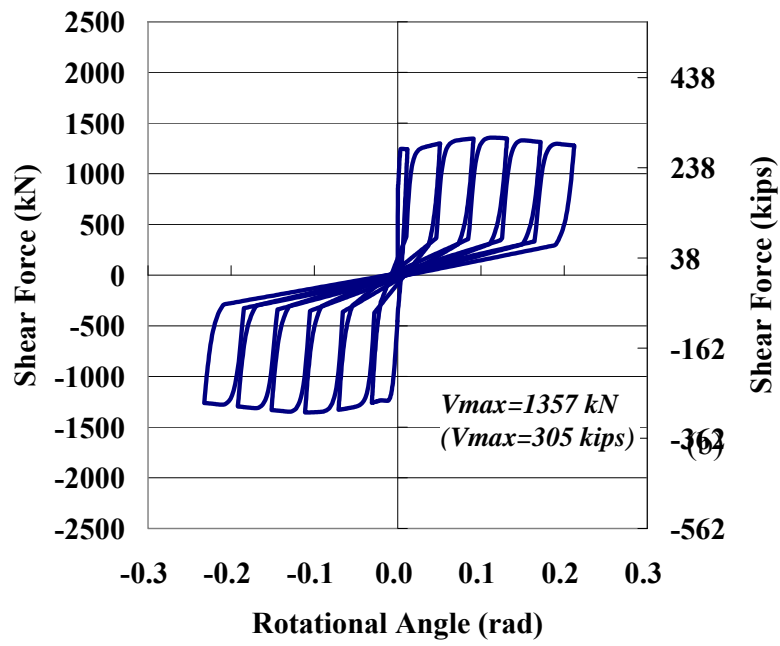
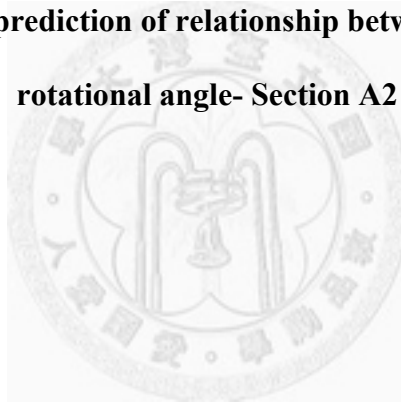


Fig. 24—Analytical prediction of relationship between shear force and rotational angle- Section A2



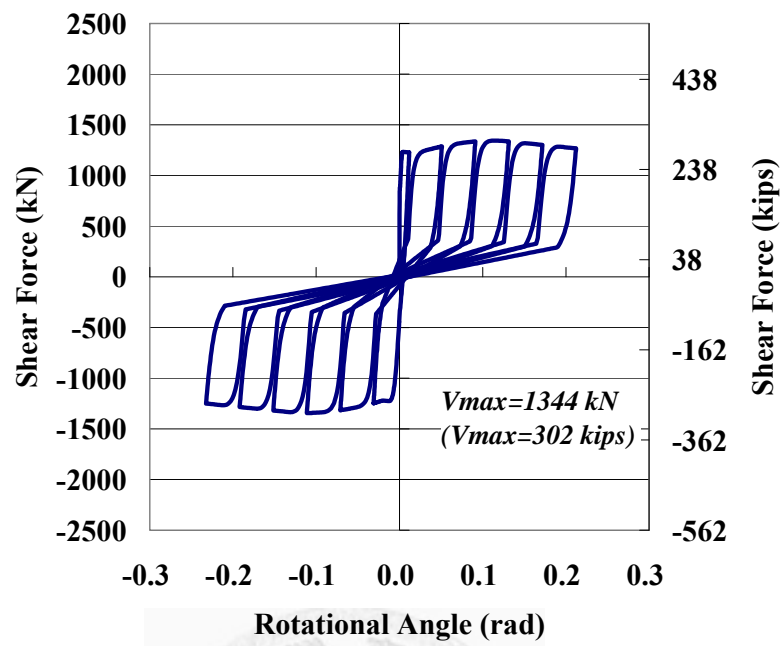


Fig. 25—Analytical prediction of relationship between shear force and rotational angle- Section B1

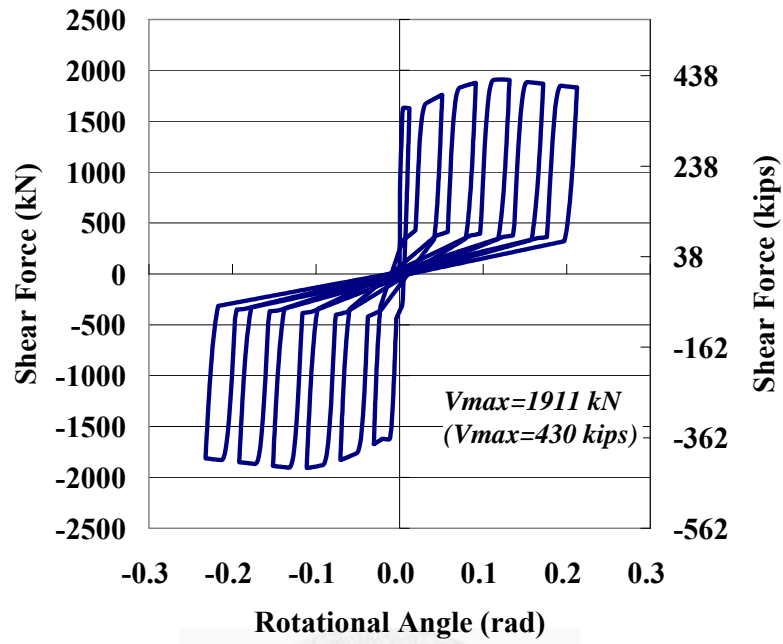


Fig. 26—Analytical prediction of relationship between shear force and rotational angle- Section B2

traditional code vs. OpenSEES

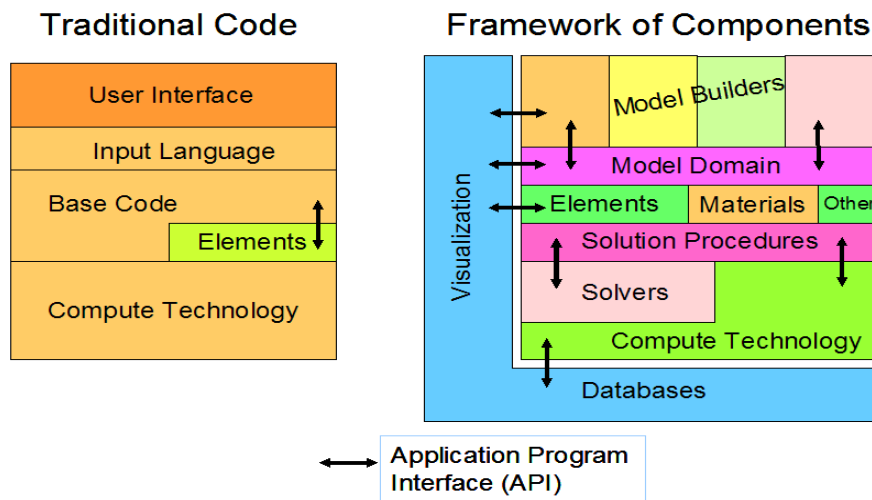


Fig. 27–Framework of OpenSees.



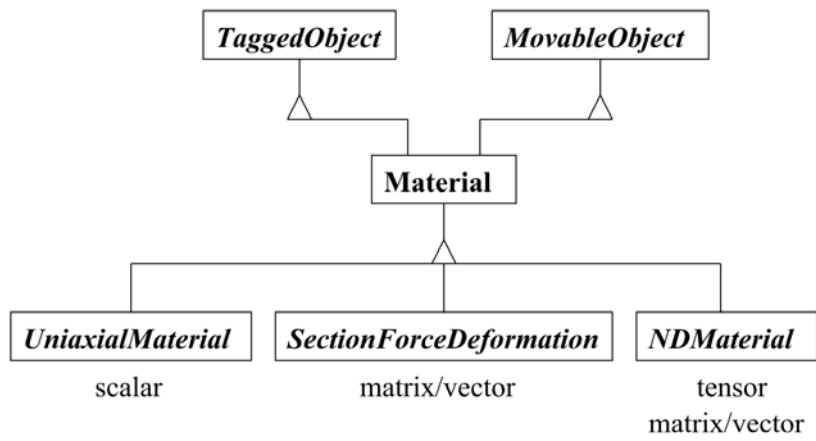
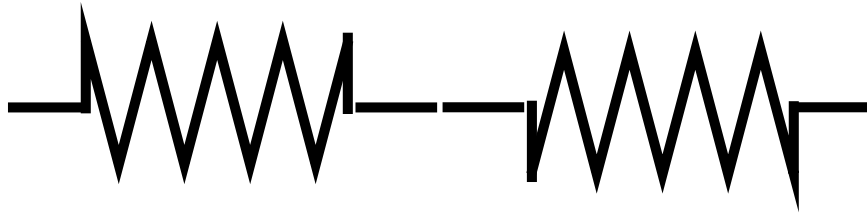


Fig. 28–Material class hierarchy. [14]



Shear Model



Flexural Model

Fig. 29–Flexural and shear models connected in series.



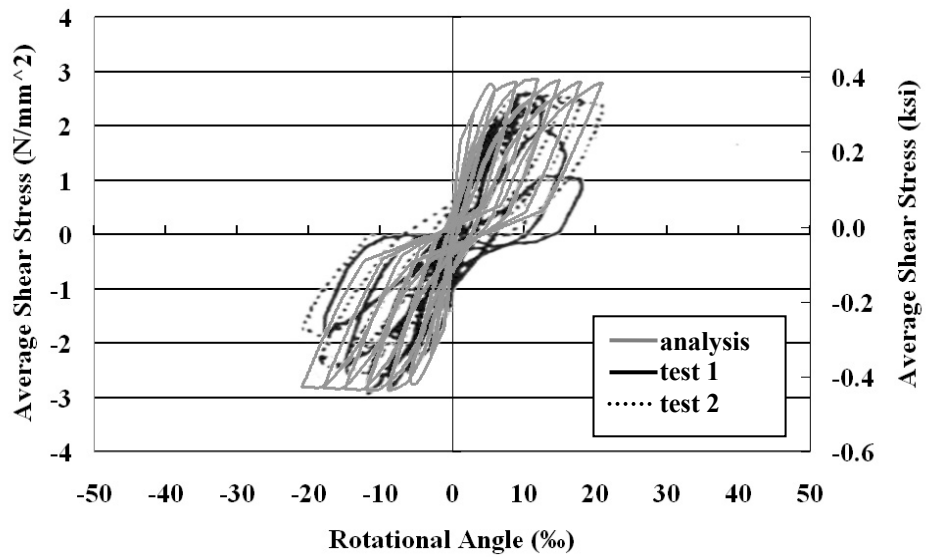
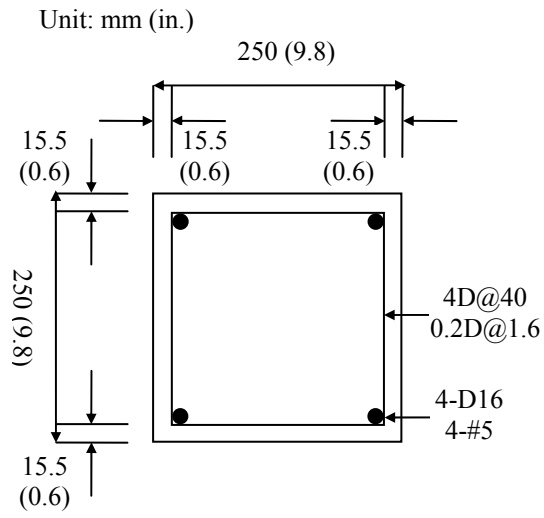


Fig. 30—Comparison of analytical and test results for specimen SY.

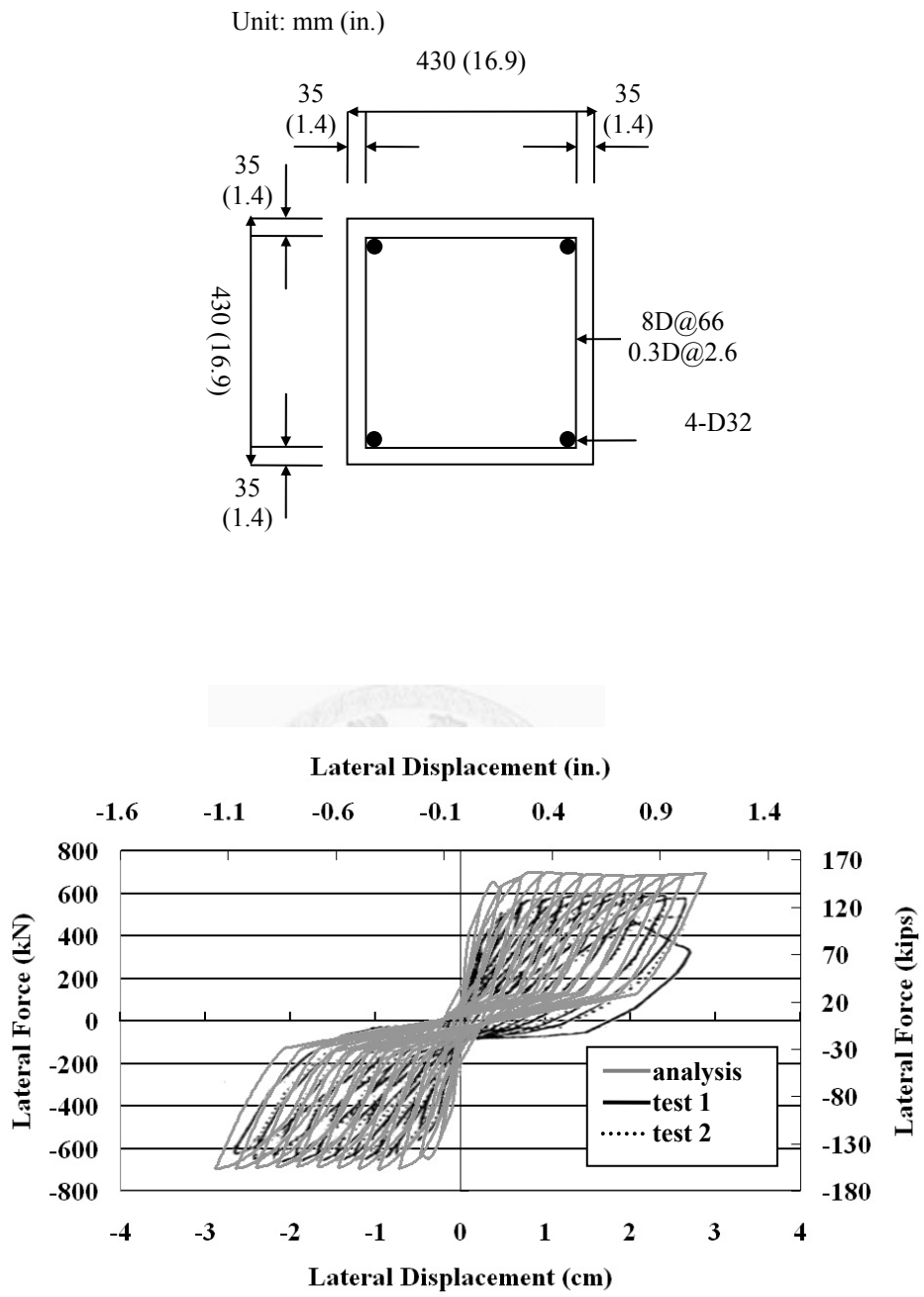


Fig. 31–Comparison of analytical and test results for specimen LY.

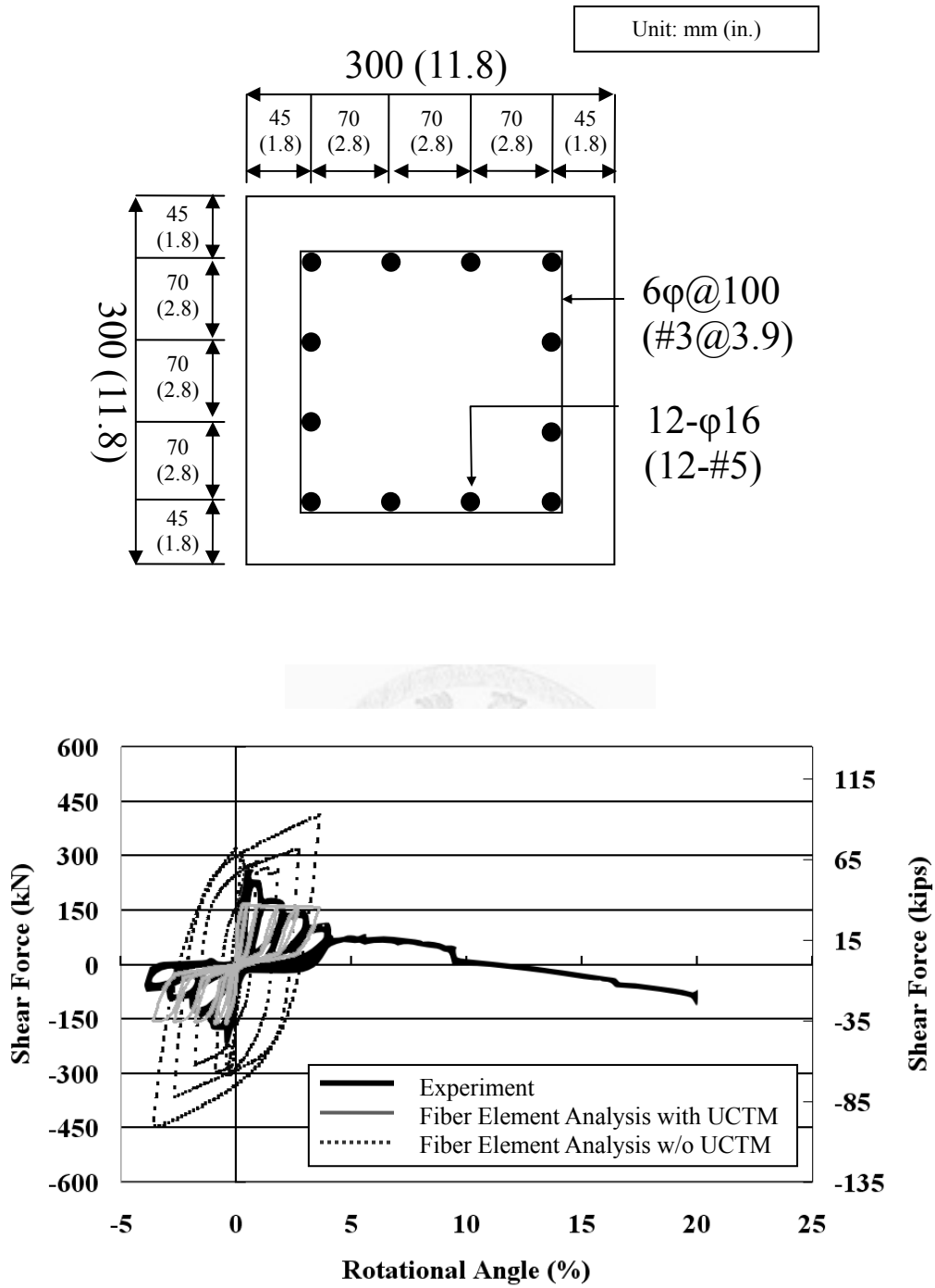


Fig. 32–Comparison of analytical and test results for specimen N18C.

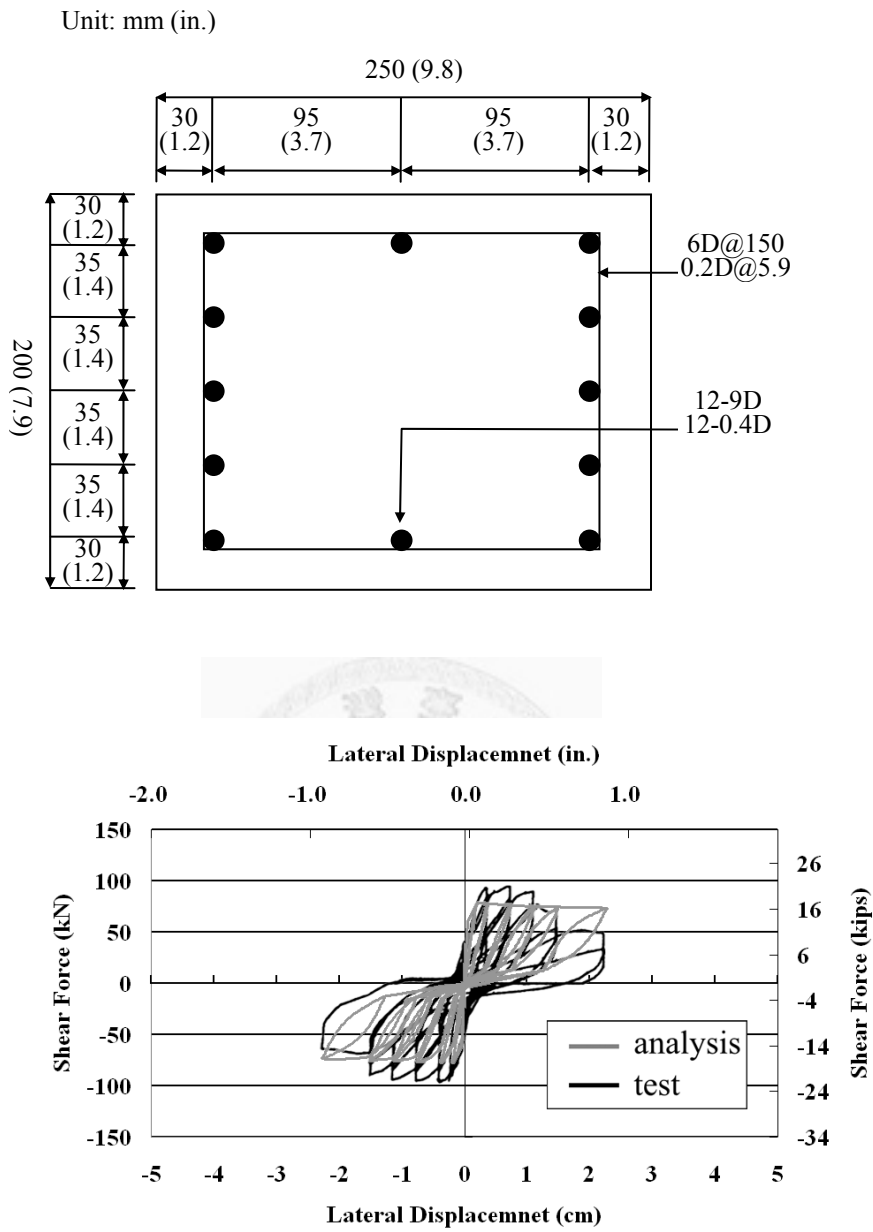


Fig. 33—Comparison of analytical and test results for specimen H-19.

Unit: mm (in.)

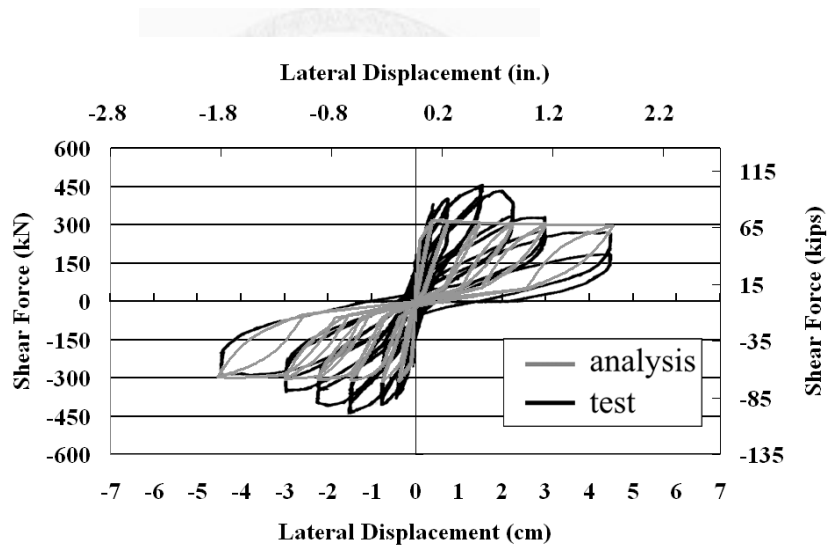
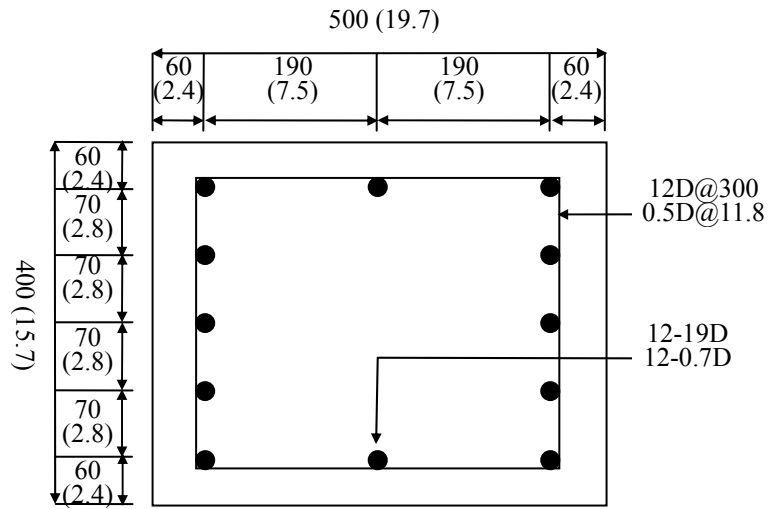


Fig. 34–Comparison of analytical and test results for specimen F-19.

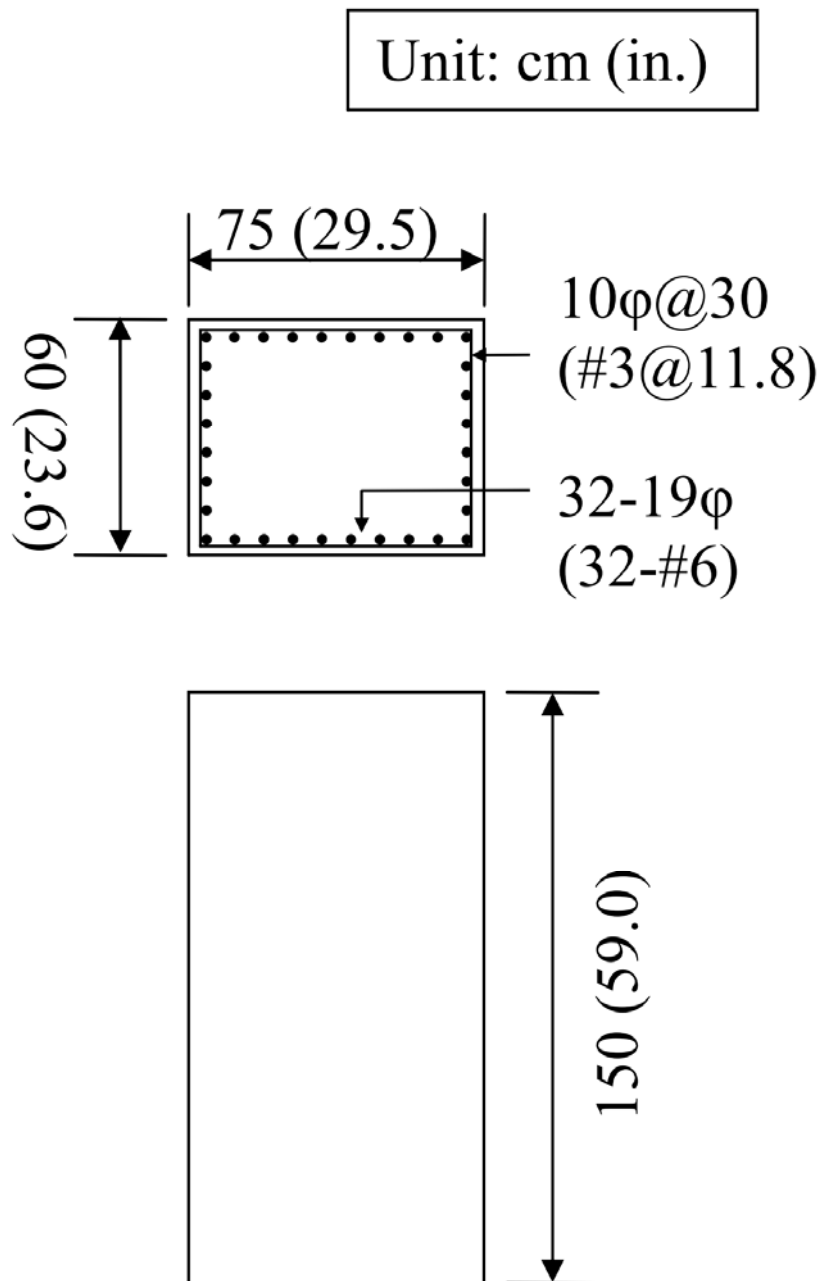
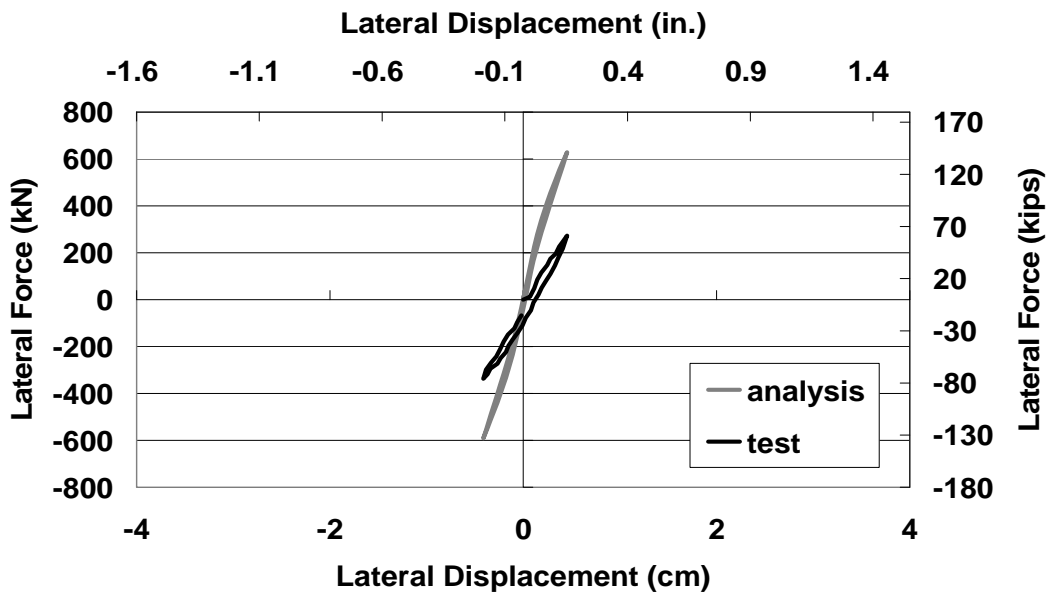
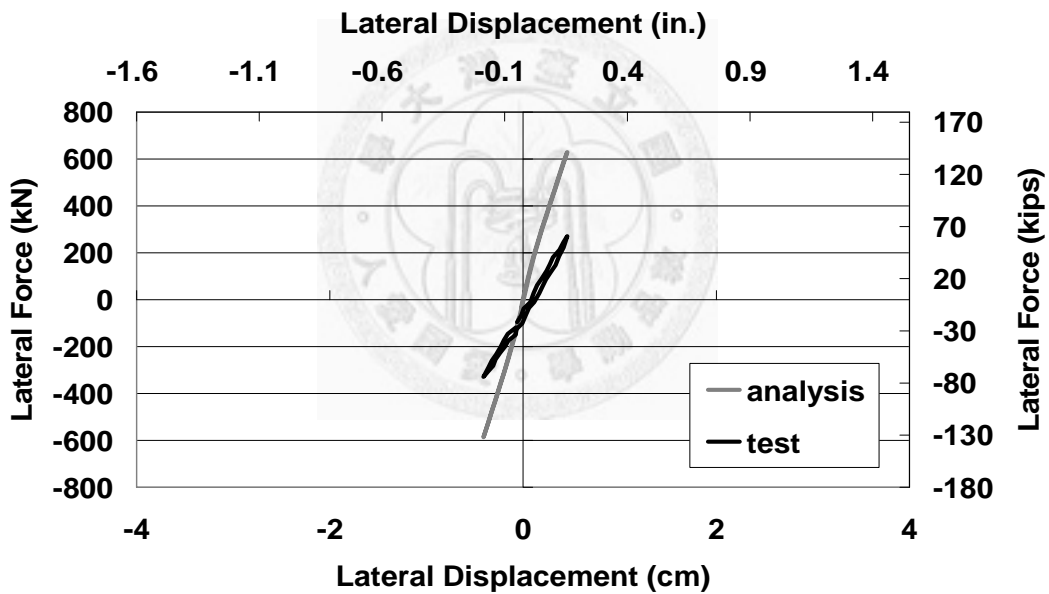


Fig. 35–Lateral View of experimental configuration of specimen BMRS.



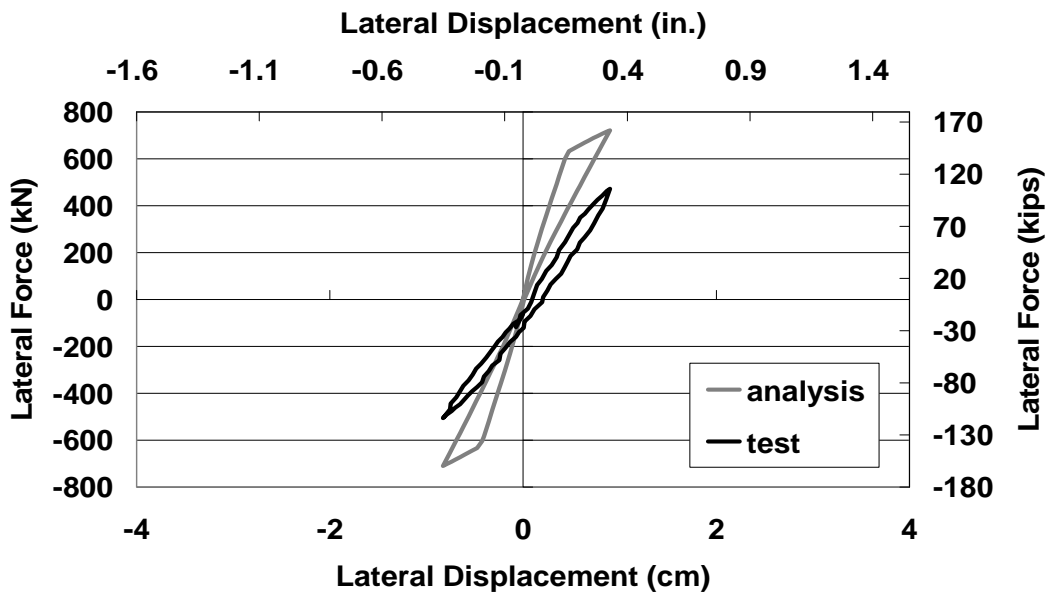
(a)



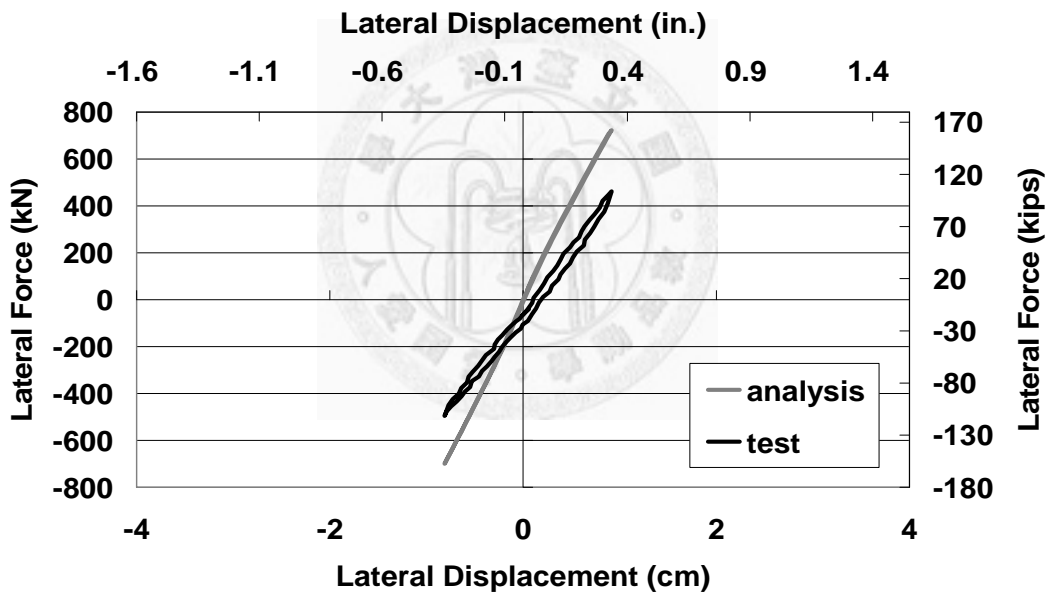
(b)

Fig. 36—Comparison of analytical and experimental hysteretic loops associated with lateral force-displacement relationship of specimen BMRS for cycles 1-2:

(a) cycle 1 (b) cycle 2.



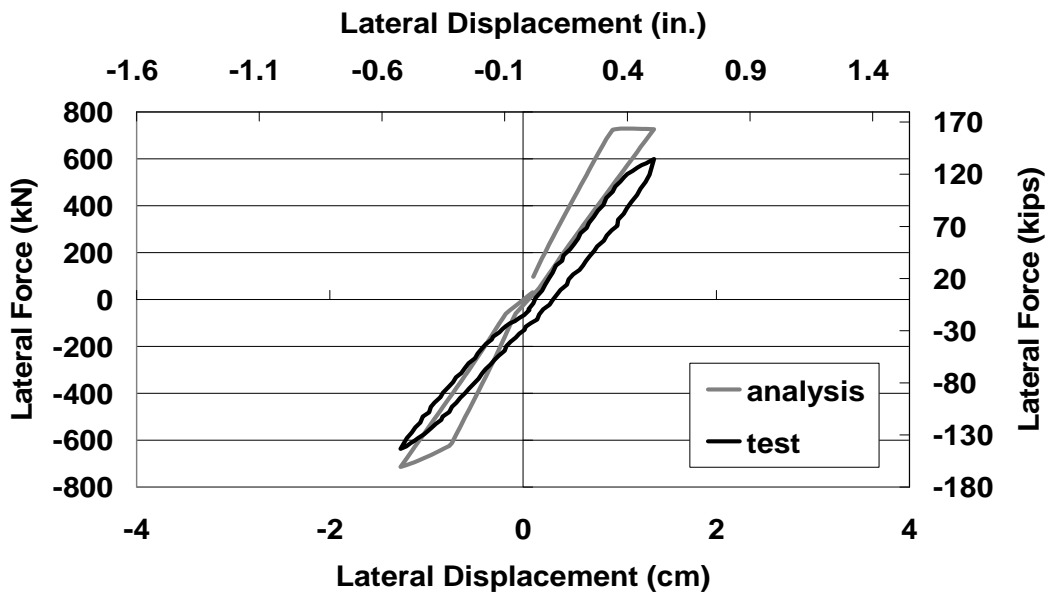
(a)



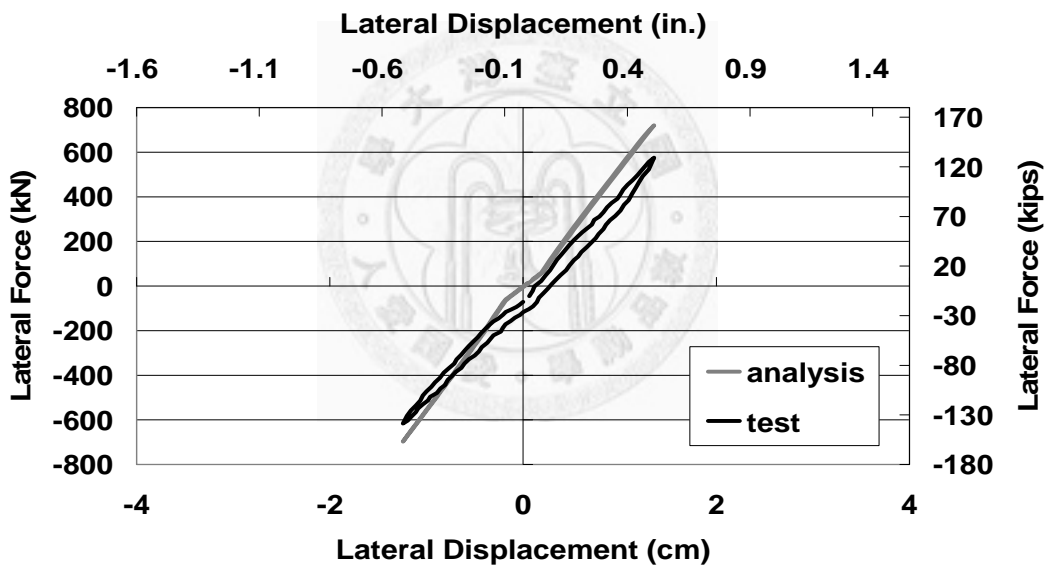
(b)

Fig. 37–Comparison of analytical and experimental hysteretic loops associated with lateral force-displacement relationship of specimen BMRS for cycles 3-4:

(a) cycle 3 (b) cycle 4.



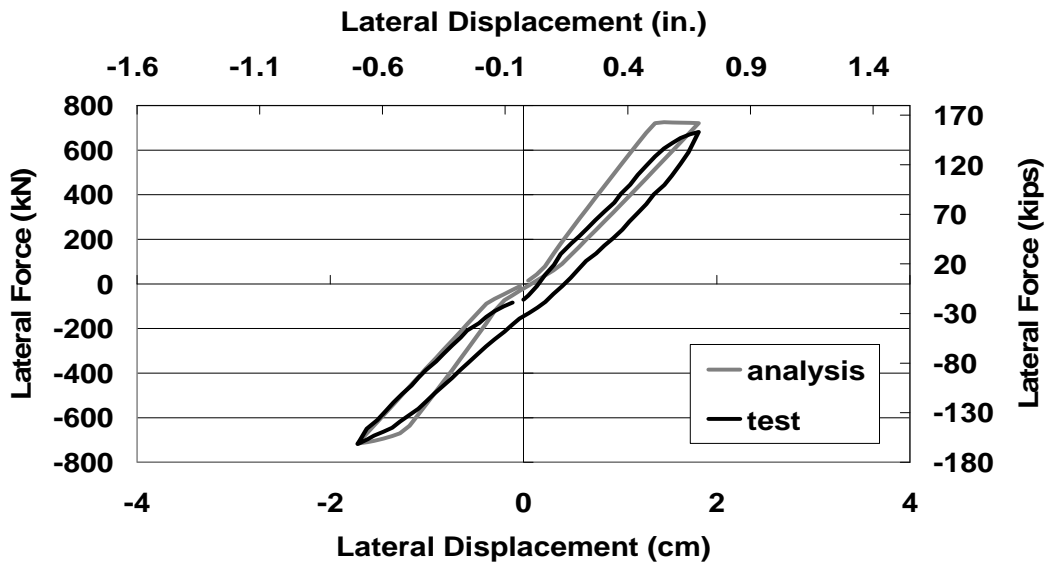
(a)



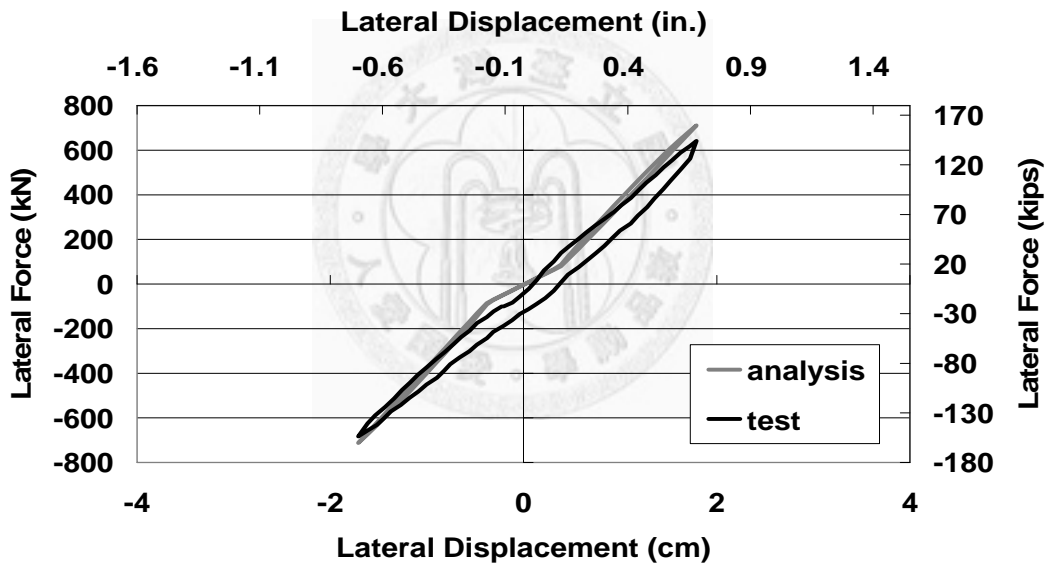
(b)

Fig. 38—Comparison of analytical and experimental hysteretic loops associated with lateral force-displacement relationship of specimen BMRS for cycles 5-6:

(a) cycle 5 (b) cycle 6.



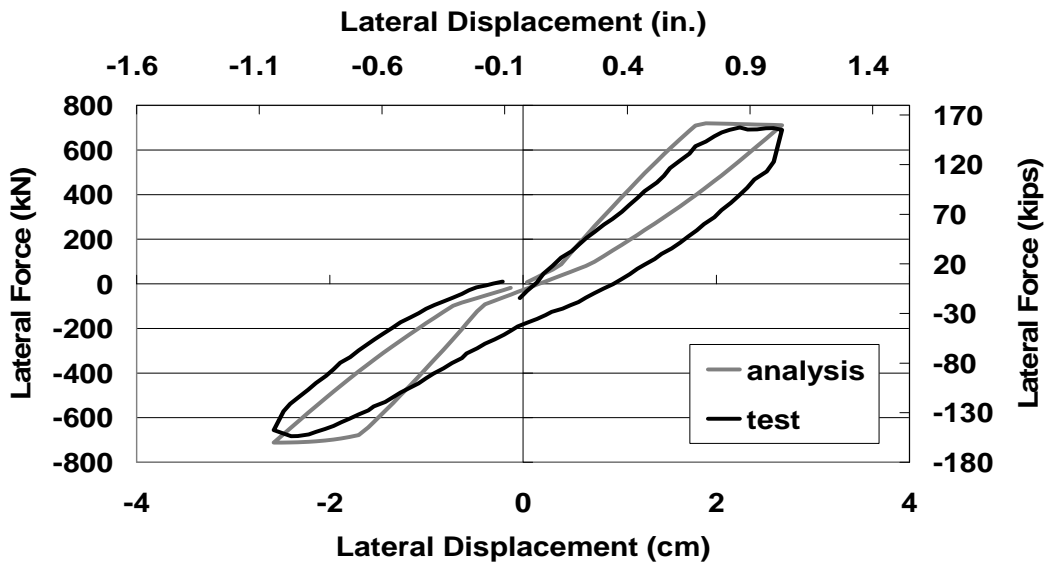
(a)



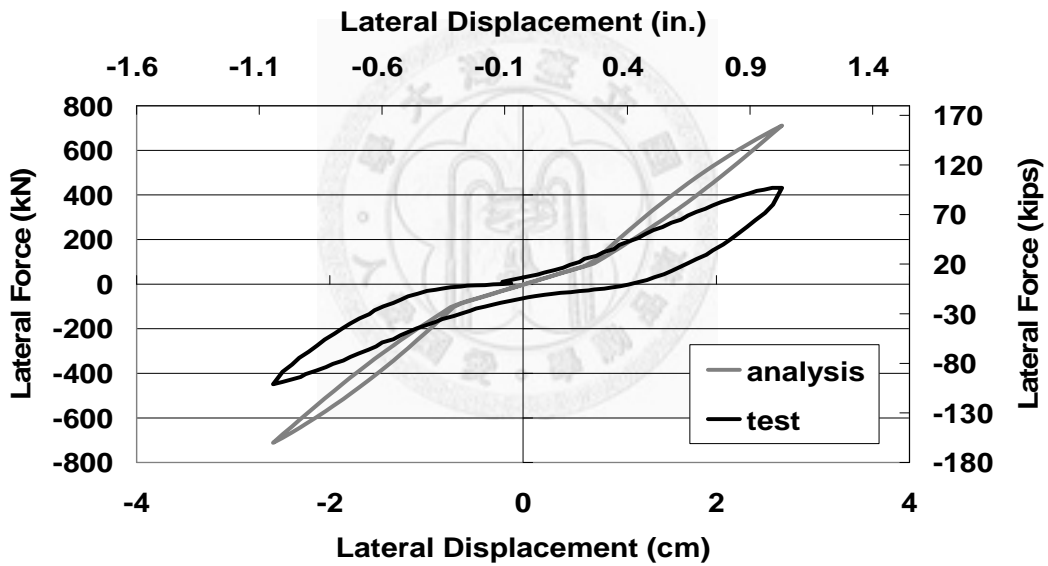
(b)

Fig. 39–Comparison of analytical and experimental hysteretic loops associated with lateral force-displacement relationship of specimen BMRS for cycles 7-8:

(a) cycle 7 (b) cycle 8.



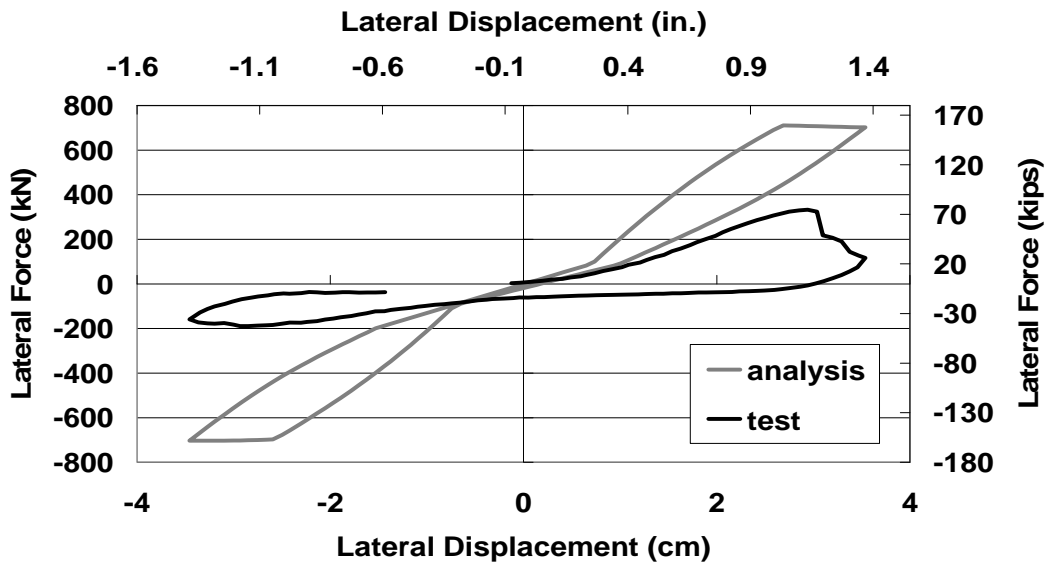
(a)



(b)

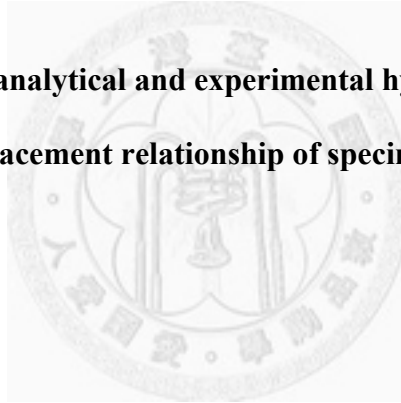
Fig. 40—Comparison of analytical and experimental hysteretic loops associated with lateral force-displacement relationship of specimen BMRS for cycles 9-10:

(a) cycle 9 (b) cycle 10.



(a)

Fig. 41–Comparison of analytical and experimental hysteretic loops associated with lateral force-displacement relationship of specimen BMRS for cycle 11.



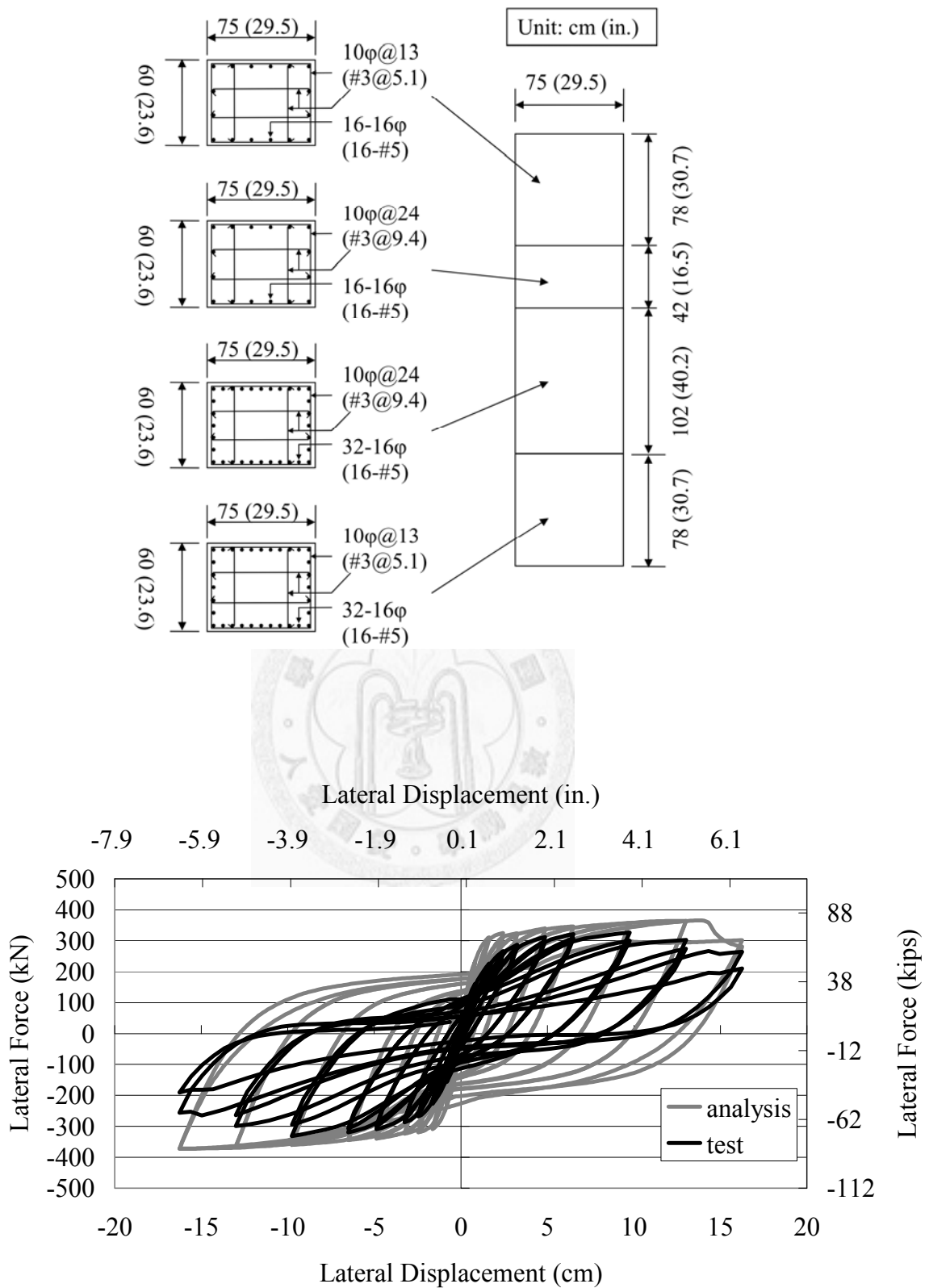


Fig. 42–Comparison of analytical and experimental lateral force-displacement hysteretic loops for specimen BMR2.